JCI The Journal of Clinical Investigation

Factors associated with resistance of HIV-1 reservoir viruses to neutralization by autologous IgG antibodies

Natalie F. McMyn, … , Janet M. Siliciano, Robert F. Siliciano

J Clin Invest. 2025. https://doi.org/10.1172/JCI194081.

Clinical Research and Public Health In-Press Preview **AIDS/HIV** **Infectious disease** **Virology**

Antiretroviral therapy (ART) prevents HIV-1 replication but does not eliminate the latent reservoir, the source of viral rebound if treatment is stopped. Autologous neutralizing antibodies (aNAbs) can block in vitro outgrowth of a subset of reservoir viruses and therefore potentially affect viral rebound upon ART interruption. We investigated aNAbs in 31 people with HIV-1 (PWH) on ART. Participants fell into two groups based on a high or low fraction of aNAb-resistant reservoir isolates, with most isolates being aNAb-resistant (IC_{50} >100 μg/ml). Time on uninterrupted ART was associated with higher aNAb resistance. However, pharmacodynamic analysis predicted that many isolates would be partially inhibited at physiologic IgG concentrations, to the same degree as by single antiretroviral drugs. Steep dose-response curve slopes, an indication of cooperativity, were observed for the rare isolates that were very strongly inhibited (>5 logs) by aNAbs. Resistance to aNAbs was not fully explained by declining in aNAb titers and may be driven partially by ADCC-mediated elimination of infected cells carrying aNAb-sensitive viruses over long time intervals, leaving only aNAb-resistant viruses which can contribute to viral rebound.

Factors associated with resistance of HIV-1 reservoir viruses to neutralization by autologous IgG antibodies

Natalie F. McMyn[1,] Joseph Varriale[1], Hanna W. S. Wu[1], Vivek Hariharan[1], Milica Moskovljevic[1], Toong Seng Tan[2], Jun Lai[1], Anushka Singhal[1], Kenneth Lynn[3,4], Karam Mounzer[5], Pablo Tebas[4], Luis J. Montaner[3], Rebecca Hoh[6], Xu G. Yu[2], Mathias Lichterfeld[2], Francesco R. Simonetti[1], Colin Kovacs[7], Steven G. Deeks[6], Janet M. Siliciano[1], and Robert F. Siliciano[1,8]

[1]Johns Hopkins University School of Medicine, Baltimore, Maryland, USA

[2]Brigham and Women's Hospital, Boston, Massachusetts, USA; Ragon Institute of MGH, MIT and Harvard, Cambridge, Massachusetts, USA.

[3]The Wistar Institute, Philadelphia, Pennsylvania, USA

[4]University of Pennsylvania, Philadelphia, Pennsylvania, USA

[5]Philadelphia Field Initiating Group for HIV-1 Trials, Philadelphia, Pennsylvania, US

[6] University of California San Francisco, San Francisco, California, USA

[7]Maple Leaf Medical Clinic, Toronto, Ontario, CAN

[8]Howard Hughes Medical Institute, Baltimore, Maryland, USA

*Corresponding author: Dr. Robert Siliciano, Department of Medicine, Johns Hopkins University School of Medicine, 733 N. Broadway, Baltimore MD 21205

Email: rsiliciano@jhmi.edu Phone: 4109552958

RFS is an inventor on a patent application for the intact proviral DNA assay (IPDA) filed by JHU and licensed by AccelevirDx.

Abstract

Antiretroviral therapy (ART) prevents HIV-1 replication but does not eliminate the latent reservoir, the source of viral rebound if treatment is stopped. Autologous neutralizing antibodies (aNAbs) can block in vitro outgrowth of a subset of reservoir viruses and therefore potentially affect viral rebound upon ART interruption. We investigated aNAbs in 31 people with HIV-1 (PWH) on ART. Participants fell into two groups based on a high or low fraction of aNAb-resistant reservoir isolates, with most isolates being aNAb-resistant (IC_{50} >100 μg/ml). Time on uninterrupted ART was associated with higher aNAb resistance. However, pharmacodynamic analysis predicted that many isolates would be partially inhibited at physiologic IgG concentrations, to the same degree as by single antiretroviral drugs. Steep dose-response curve slopes, an indication of cooperativity, were observed for the rare isolates that were very strongly inhibited (>5 logs) by aNAbs. Resistance to aNAbs was not fully explained by declining in aNAb titers and may be driven partially by ADCC-mediated elimination of infected cells carrying aNAb-sensitive viruses over long time intervals, leaving only aNAb-resistant viruses which can contribute to viral rebound.

Introduction

The major barrier to HIV-1 cure is a population of latently infected resting $CD4^+$ T cells which harbor replication-competent proviruses but are protected from immune clearance by viral latency (1–5). Antiretroviral therapy (ART) blocks new infection events but does not eliminate this latent reservoir (6–8). Upon ART interruption, viruses from the reservoir cause rebound viremia, typically within weeks (9–11). The reservoir decays slowly ($t_{1/2}$=44 months) over the first seven years of ART (12–14), but then increases slowly (t_2 = 23 years) (15) due to infected cell proliferation (15–24) driven largely by antigen (25–29). In people with HIV-1 (PWH), particularly those on ART for >20 years, the reservoir is dominated by large clones of infected cells (15, 21–23). Importantly, autologous neutralizing antibodies (aNAbs) prevent rebound from a substantial but variable fraction of reservoir viruses, even those in large clones (30).

aNAbs target the HIV-1 envelope (Env) trimer on the virion surface and the plasma membrane of infected cells (31). Neutralization involves antibody binding to virions via Fab regions in a way that interferes with viral entry and thus blocks new infection events (32). Other antiviral activities of antibodies are mediated by Fc-dependent effector functions (33). HIV-1 has mechanisms to evade neutralization. Env is heavily glycosylated (34), and critical functional regions are shielded by five variable regions. Conserved antibody epitopes are rendered inaccessible through steric hindrance (35) and conformational masking (36). Another important mechanism is the rapid accumulation of mutations, which reflects the high error rate with which HIV-1 reverse transcriptase copies the viral genome in newly infected cells (37) and the high number of new infection events occurring daily during untreated infection (38, 39). Mutations accumulating in the five variable regions of the gp120 subunit of Env include point mutations, some of which alter the Env glycan shield (34), and insertions and deletions that range from one to several amino acids. The swift evolution of escape variants (40–42) enables HIV-1 to overcome circulating contemporaneous aNAbs as they arise.

Since aNAbs target variable regions and are thus largely strain-specific, vaccine efforts have focused on broadly neutralizing antibodies (bNAbs) (43–46) which block entry of HIV-1 strains from different PWH (44, 45, 47). While aNAbs are induced within 2-3 months after infection in most PWH (41–43, 48), bNAbs only arise in a subset of PWH after extensive somatic hypermutation, which can take months to years (49–52). Administration of bNAbs can delay viral rebound after ART interruption (53–57). However, viremia typically rebounds when bNAb concentrations fall to subinhibitory levels. bNAbs can also target infected cells through antibody-dependent cellular cytotoxicity (ADCC) (58–60). Most bNAb trials in PWH have not produced reservoir reduction, likely because latently infected cells do not express viral proteins (57, 61, 62). However, in one trial, a 46% reduction was measured by Q4PCR (55).

Recent studies suggest that selection can operate on reservoir cells. Cells carrying intact proviruses decay faster than cells carrying defective proviruses during the first years of ART, possibly reflecting immune mechanisms targeting cells with transcriptionally active, intact proviruses (63, 64). Similarly, while proviruses are typically integrated within active genes (65, 66), an increased fraction of intact proviruses in intergenic regions and chromosomal locations repressive for transcription is reported in PWH initiating ART early (67), PWH on long-term ART (68), and elite controllers (69). Reservoir selection through innate immune mechanisms, possibly involving NK cells, has also been reported (70–72). Thus, antibodies involved in ADCC may play a role in changing reservoir composition over time. Furthermore, immune pressure from aNAbs has been seen in multiple studies. Viruses rebounding after treatment interruption were more resistant to aNAbs, possibly reflecting aNAb-mediated inhibition of outgrowth of sensitive viruses (30, 73, 74). Together, these findings indicate that over time, reservoir composition may be altered by both the clonal expansion of infected cells and selection against cells expressing viral antigens.

Given that rebound from some reservoir viruses is blocked by aNAbs (30), we examined the neutralizing activity of contemporaneous autologous IgG antibodies against inducible, replication-competent HIV-1 isolates from a large cohort of PWH on ART, including many who had had stable suppression of viremia for 20-25 years. We defined the extent and durability of aNAb responses. We also investigated antibody-based selection against cells carrying aNAb-sensitive viruses.

Results

Study participants. We studied 31 PWH, including 9 participants from our initial aNAb study (30) who had extensive reservoir sequencing. The mean time on combination ART was 15.9 years (range 4.5-26.7 years, Supplemental Table S1). The demographics were 87.1% male, 64.5% Black, 32.3% White, and 3.2% Pacific Islander. Participants had a mean CD4 nadir of 225 cells/µl and a mean age of 54 years at the last sample collection. Viral outgrowth results for 25 participants were previously reported in Bertagnolli et al. (30) and McMyn et al. (15). Those studies showed that replication-competent virus could be readily isolated from study participants, even those on ART for >20 years, at frequencies between 0.05-16.25 infectious units per million (IUPM) resting $CD4^+$ T cells, and that aNAbs could suppress outgrowth of a subset of these viruses.

All participants initiated ART during chronic infection. Longitudinal plasma HIV-1 RNA levels and CD4 counts are in Supplemental Figure 1 and McMyn et al. (15). Five participants had short periods of ART interruption. Three of these (DEL-SPC-015, -017, and -019) were in ACTG clinical trial A5340 (IDs A02, A06, and A13, respectively) which involved administration of the bNAb VRC01 and an analytic treatment interruption (ATI). Plasma HIV-1 RNA levels during the ATI were previously reported (54). DEL-SPC-012 and JH448 had treatment interruptions due to non-adherence. All participants had plasma HIV-1 RNA levels below the detection limit (<20–40 copies/ml) at the time of sampling. Small, isolated blips, transient increases in HIV-RNA above the detection limit (75, 76), were not considered in calculating time on uninterrupted ART.

Sensitivity of reservoir isolates to aNAbs. To determine the aNAb sensitivity of replication-competent proviruses from a diverse group of PWH, we performed quantitative viral outgrowth assays (QVOAs) (77, 78) using resting $CD4^+$ T cells. Cultures from 28/31 participants had ≥5 $p24^+$ outgrowth wells, for a total of 591 independent isolates. Full length *env* sequencing revealed 138 different (distinct) *env* sequences. The other 453 sequences were identical to other sequences from the same participant. Among sequences found more than once, there were 69 sets of identical sequences ranging in size from 2 to 59 isolates. Distinct *env* sequences were cloned into expression vectors for pseudovirus generation and neutralization assays as previously described (30). Because non-specific inhibition can be observed at IgG concentrations >100 μg/ml, we arbitrarily designated isolates as resistant if the IC_{50} for autologous IgG was >100 μg/ml.

Of 138 distinct HIV-1 Env pseudoviruses from 28 PWH 55% (76/138) were resistant to neutralization (Figure 1A). Since some individuals had fewer distinct isolates to test due to high reservoir clonality and/or smaller reservoir size, we determined the fraction of resistant isolates per PWH to normalize for different numbers of isolates per participant (Figure 1B). There was wide variation in the fraction of resistant sequences (0-100%, median 80%).

Effects of reservoir clonality. The analyses presented above consider only distinct variants. However, reservoir composition is also influenced by clonal expansion. Therefore, we analyzed resistance to aNAbs considering all isolates from each donor, not just distinct sequences. Of 591 total isolates, 60% (357/591) were resistant to contemporaneous aNAbs (IC_{50} >100 μg/ml, Figure 1C). After normalizing for different numbers of isolates for each participant, we found a median of 92% resistant viruses per PWH, again with very high person-to-person variation (0-100%) (Figure 1D). For 43% of participants, all reservoir isolates were resistant (Figure 1, B and D).

Factors associated with aNAb resistance. Figure 1D reveals a separation in aNAb resistance between 20 participants with high resistance (67-100% resistant isolates per PWH) and 8 participants with high sensitivity (0-26% resistant isolates per PWH). Of 74 distinct viral isolates from the high resistance group, 64 isolates (86%) were neutralization-resistant (Figure 2A). This fraction was significantly higher than the 19% observed in the group with high aNAb sensitivity (12/64 distinct aNAb-resistant isolates, $P < 0.0001$, Figure 2A). The difference was visually apparent in flatter neutralization curves for the aNAb-resistant group (Figure 2, B and C). The impact of dose-response curve slope is described below. For both groups, resistant variants were found among sets of isolates with identical *env* sequences as well as sequences observed only once (Supplemental Figures 2 and 3). There were no correlations between aNAb IC_{50} values and the number of identical sequences in a set for either group (Supplemental Figure 4).

We next explored other explanations for differences in aNAb resistance. No significant differences between the two groups were found for CD4 nadir, a proxy for time of untreated infection (Supplemental Figure 5A), or reservoir size based on QVOA measurements (Supplemental Figure 5B). We then evaluated differences in total time on ART. Although the mean time on ART for the aNAb-resistant group was higher (16.9 vs. 10.9 years), the difference was not significant ($P = 0.1018$, Supplemental Figure 5C). This time included the time that five participants (DEL-SPC-012, -015, -017, -019, and JH448) experienced treatment interruptions. Therefore, we compared time on uninterrupted ART, or time since last period of measurable viremia. This analysis resulted in significant differences. For the aNAb-resistant group, the average time of uninterrupted ART was 16.5 years, significantly higher than the average time of 8.2 years for the aNAb-sensitive group ($P = 0.0277$, Supplemental Figure 5D). These results suggest that ART interruptions and shorter times on uninterrupted ART may affect neutralization sensitivity.

To further investigate the relationship between aNAb resistance and time on ART, we analyzed the correlation between aNAb IC_{50} values or % resistance per person and time on ART or time on uninterrupted ART. There was a significant positive correlation between the aNAb IC_{50} values of distinct isolates from both the aNAb-sensitive and aNAb-resistant groups and time on ART (Spearman r = 0.2058, P = <0.0155; Supplemental Figure 6A). We found a more significant positive correlation between aNAb IC_{50} values of distinct isolates and time on uninterrupted ART (Spearman r = 0.4644, P = <0.0001, Supplemental Figure 6B). When the analysis was expanded to include all independent isolates from each PWH and not simply the distinct isolates, the correlation was highly significant for both time on ART (Spearman r = 0.2441, P = <0.0001) and time on uninterrupted ART (Spearman r = 0.3909, P = <0.0001. Because these analyses are affected by the number of isolates per donor, we also examined the correlation between the fraction of distinct isolates that were resistant in each PWH and the time on uninterrupted ART. We found a significant positive correlation (Spearman r = 0.5154, P = 0.0050; Figure 2D). When the analysis included all isolates from each PWH, including identical sequences, there was a weaker positive correlation (Spearman r = 0.4327, P = 0.0215, Figure 2E). When the total time on ART was used, no significant correlation was found. Although conclusions depended on how time on ART was defined, longer times on ART were generally associated with greater aNAb resistance, perhaps indicating gradual selection against cells carrying aNAb-sensitive viruses (see below).

To determine whether the observed aNAb resistance of replication-competent isolates was representative of other persistent proviruses not detected in outgrowth assays, we assessed aNAb sensitivity of intact *env* sequences amplified from resting $CD4^+$ T cells from six PWH on long-term ART (>21 years) (15). The high aNAb resistance of outgrowth viruses was also observed for these proviruses (Supplemental Figure 2). Across the six participants, 16 of 17 distinct proviruses were resistant. The one sensitive isolate had an IC_{50} of 96.12 μg/ml. These results provide evidence for a latent reservoir dominated by resistant variants regardless of inducibility. The finding that most reservoir viruses are resistant to neutralization by contemporaneous IgG, especially in PWH on long-term ART, suggests that over long time intervals, there may be a selection against cells carrying aNAb-sensitive viruses. Alternatively, a decline in aNAb concentration may explain reduced neutralization (see below).

aNAb resistance at physiologic IgG concentrations. The above results indicate that in many PWH on ART, most replication-competent reservoir viruses are not strongly neutralized by contemporaneous autologous IgG in in vitro assays. However, these assays are carried out using polyclonal IgG concentrations in the µg/ml range while the in vivo plasma concentration of IgG is 7-16 mg/ml (79). From conventional dose-response curves, it is difficult to ascertain the degree of inhibition at in vivo concentrations (Figure 3A). Therefore, we used previously described pharmacodynamic metrics to predict the in vivo effects of aNAbs (80–82). The dose response curve can be described using the median effect equation (83):

$$\frac{(1-f_u)}{f_u} = \left(\frac{c}{IC_{50}}\right)^m$$

where f_u is the fraction of infection events unaffected (not inhibited) by antibodies at concentration (*c*) given the IC_{50} and the dose response curve slope *(m)* or Hill coefficient, a measure of cooperativity that is equal to 1 for non-cooperative processes. Slopes >1 give steeper dose-response curves, but differences in inhibition at physiologic IgG concentrations are only apparent if the y-axis values are displayed on a log scale (Figure 3B). The inverse of this plot gives the instantaneous inhibitory potential (IIP),

$$IIP = \log\left(\frac{1}{f_u}\right) = \log\left(1 + \left(\frac{c}{IC_{50}}\right)^m\right)$$

an intuitive metric of antiviral activity which is the number of logs by which single round infection events are reduced at a given antibody concentration (Figure 3C) (80–82). IIP depends on both IC_{50} and *m* (Figure 3D). Because of their exponential relationship, IIP is strongly influenced by *m*. Figure 3D shows calculated IIP at 10 mg/ml of IgG based on experimental measurements of IC_{50} and *m* for distinct isolates from the aNAb-resistant and aNAb-sensitive groups. As expected, IIP values are strongly influenced by *m* (linear regression R^2 = 0.77 and 0.83 for isolates from the resistant and sensitive groups, respectively). Figure 3E shows slope values for the two groups. Although antigenic and antibody heterogeneity can reduce slope, we observed slopes >1, indicative of positive cooperativity, as is seen for HIV-1 protease inhibitors, non-nucleoside reverse transcriptase inhibitors, entry inhibitors, and some bNAbs (80–82, 84).

This analysis allows extrapolation of dose-response curves to physiologic IgG concentrations (Figure 3F). For the aNAb-resistant group, most isolates were weakly inhibited with a median IIP of 1.3, just above the level of non-specific inhibition observed with control IgG. For the aNAb-sensitive group, many isolates were inhibited with a median IIP of 2.4, meaning >2 logs of inhibition at in vivo IgG concentrations, comparable to single antiretroviral drugs (80–82). Effective combination ART regimens produce >5 logs of inhibition (85). Only four isolates were inhibited by aNAbs with IIP >5 (Figure 3F). These isolates had IC_{50} values <13 μg/ml and slopes >1.7 (Supplemental Table 2). This analysis excluded 43 distinct isolates from the aNAb-resistant group and 16 from the aNAb-sensitive group because slopes and IIP values could not be calculated due to poor inhibition (non-decreasing dose response curves, maximum inhibition <20%, or median effect plot R^2 <0.8). Together, these results indicate that like single antiretroviral drugs, aNAbs can reduce replication of many reservoir viruses but not sufficiently to prevent selection of resistant variants.

Sensitivity of reservoir viruses to neutralization by bNAbs. In light of the high proportion of aNAb-resistance after long-term ART, we explored whether these viruses were resistant to three clinically relevant bNAbs: VRC01, 10-1074, and PGDM1400, which bind to the CD4 binding site, the V3 glycan site, and the V2 apex, respectively (45). Many isolates from the aNAb-resistant group were neutralized by bNAbs (median bNAb IC_{50}: 1.280, 2.857, and 1.595 μg/ml for VRC01, 10-1074, and PGDM1400, respectively; Figure 4A). For 90% of donors in the aNAb-resistant group, all isolates were sensitive to at least one bNAb with IC_{50} values <4 µg/ml, and 55% of donors had isolates sensitive to at least two bNAbs (Supplemental Table 3). Thus, although viral isolates from these PWH were aNAb-resistant, many isolates were sensitive to neutralization by one or more bNAbs. Only four isolates from two PWH were resistant to all three bNAbs. Importantly, bNAb sensitivity was not a predictor of aNAb sensitivity. The 10 isolates with aNAb IC_{50} values <100 µg/ml had similar bNAb sensitivities to isolates with aNAb IC_{50} values >100 µg/ml (Supplemental Table 3). Ultimately, the majority of viruses in the aNAb-resistant group could be effectively neutralized by some bNAbs, ruling out general neutralization resistance as an explanation for high aNAb-resistance in that group. Similar results were obtained for the aNAb-sensitive group (Figure 4B).

Some aNAb responses persist over long times on ART. Another explanation for the large proportion of outgrowth viruses resistant to aNAbs is that without antigen, the anti-HIV antibody response wanes. Therefore, we studied antibody responses in participants on very long-term ART. Western blot analysis of IgG from a set of participants who had been on ART for an average of 22.6 years showed that some anti-HIV antibodies persisted despite prolonged suppression of viremia (Supplemental Figure 7). To examine whether neutralizing antibody responses persist, we first tested neutralization of pseudoviruses carrying the *env* gene of HIV-1 SF162, a tier 1 virus which is highly sensitive to neutralization by antibodies from many PWH (86, 87). Neutralization assays with SF162 pseudovirus were performed with IgG from 16 participants who had been on very long-term ART (mean 22.8 years), 12 of whom were from the aNAb-resistant group. SF162 pseudovirus was neutralized by IgG from 15 of 16 participants (Figure 5, A and B). The interquartile range of IC_{50} values was 6.9-26.4 µg/ml, with a median of 18.1 µg/ml (Figure 5B). No neutralizing activity was detected with IgG from an HIV-seronegative donor. For three participants with only one or no QVOA outgrowth viruses (SCOPE2006, JH167, JH24), participant IgG neutralized SF162 pseudovirus with IC_{50} values <26 μg/ml. This suggests that a smaller reservoir did not result in reduced antibody stability over time. Together, these results demonstrate that some neutralizing antibodies to the HIV-1 Env protein are detectable in most PWH even after >20 years of treatment, regardless of reservoir size.

Antibodies that neutralize SF162 recognize an epitope that is conserved and immunogenic. Thus, these antibodies are distinct from the aNAbs, which generally show limited heterologous neutralization (30). Examining the stability of aNAb responses in PWH on long-term ART is difficult because longitudinal plasma samples spanning two decades are rarely available. To determine if aNAb titers persist over long time intervals, we identified three study participants in the aNAb-resistant group who had been on ART for >20 years and had a plasma sample from more than a decade earlier. First, we compared aNAb neutralization of SF162 between the early and 20-year IgG samples. For two participants, neutralizing activity remained similar while in one participant there was a >1 log increase in IC_{50} (Figure 5, C-E).

We then compared neutralizing activity between the early and 20-year IgG preparations against autologous outgrowth viruses from the 20-year timepoint (Figure 5, F-H). For participant SCOPE2046, 11/11 isolates had identical *env* sequences, potentially reflecting an expanded clone (Supplemental Figure 2). For this Env, the aNAb IC_{50} increased from 81.44 to >100 μg/ml over 20.9 years of ART, demonstrating some waning of the aNAb response (Figure 5F). Interestingly, neutralization of SF162 pseudovirus remained relatively stable over the same period (Figure 5C). For the second participant (SCOPE2256), 23 of 26 isolates had identical *env* sequences (Supplemental Figure 2). For this Env, modest neutralizing activity persisted over 13 years of ART (Figure 5G) as did neutralizing activity against SF162 (Figure 5D). The other two outgrowth isolates from SCOPE2256 were identical and remained resistant (IC_{50} >100 μg/ml) at both timepoints (not shown). For the third participant (SCOPE2114), one of five distinct outgrowth viruses was neutralized by IgG from the late time point (IC_{50} = 86.41 µg/ml), while IgG from 18.5 years earlier had less neutralizing activity (IC_{50} >100 µg/ml) (Figure 5H). An opposite trend was observed for neutralization of SF162 pseudovirus (Figure 5E). The other four outgrowth viruses from SCOPE2114 remained resistant (IC_{50} >100 µg/ml) at both timepoints (not shown). Together, these observations demonstrate that aNAb responses can persist, improve, or wane, depending on the individual and the viral sequence tested. The waning of aNAb responses might explain the observed neutralization resistance in some PWH on ART, but in cases where the aNAb response remains stable, it is possible that the relevant antibodies eliminate reservoir cells carrying sensitive variants, leaving only aNAb-resistant viruses.

Autologous IgG antibodies can mediate ADCC against cells infected with reservoir viruses. We next explored whether the observed prevalence of aNAb-resistant viruses reflects a selection against cells with sensitive viruses through ADCC. Only a small subset of reservoir cells are transcriptionally active at any given time, and thus this differential killing would only become apparent over long time intervals. Therefore, we studied IgG-dependent, NK cell-mediated killing of target cells expressing autologous Envs from participants on ART for >20 years. We generated replication-competent, NL4-3-based reporter viruses (NL4-3-ΔNef-eGFP) incorporating the *env* gene from participant-specific outgrowth viruses (Figure 6A). Next, we infected CEM.NKR.CCR5 cells (88), chosen to reduce nonspecific killing. The target cells were then incubated with NK cells purified from uninfected donors in the presence of participant IgG. Killing was measured as a reduction in live, GFP^+ target cells (Supplemental Figure 8). We tested aNAb-sensitive and aNAb-resistant isolates from three long-term ART participants. Minimal non-specific killing occurred in control cultures with uninfected donor IgG, in cultures without IgG, and in cultures without NK cells (Figure 6B). For both aNAb-sensitive and aNAb-resistant viruses, we found that autologous IgG could promote ADCC by NK cells (Figure 6C-E). Interestingly, at the highest IgG concentration (50 µg/ml), we observed higher ADCC against target cells expressing aNAb-sensitive Envs compared to most of the corresponding participant's aNAb-resistant Envs (Figure 6F-H). However, there was no correlation between the neutralization IC_{50} and ADCC measured as % killing at 50 µg/ml IgG (not shown). The mixture of neutralizing and non-neutralizing antibodies in purified IgG samples complicates analysis of the effect of neutralizing antibodies on ADCC, and multiple studies highlight the role of non-neutralizing antibodies in ADCC (89–92). Nevertheless, our results suggest that the ADCC activity of aNAbs may play a role in selection, providing one explanation for the high resistance to aNAbs after 20 years of ART.

Large aNAb-resistant outgrowth clones remain stable in size. Given the potential role of aNAbs in selecting against cells carrying sensitive variants, we hypothesized that large clones of infected cells carrying aNAb-resistant viruses might persist in PWH on very long-term ART. To definitively identify infected cell clones, we used matched integration site and near full-length proviral sequencing (MIP-seq) (93). Integration sites were matched to the *env* sequences of two large clones, each from a different PWH on long-term ART in the aNAb-resistant group (Figure 7A). For those two viruses, we designed a duplex ddPCR assay using primers and probes spanning the virus-host junction (integration site) as well as the HIV-1 LTR (R-U5), to determine the frequency of the clones among resting $CD4^+$ T cells (94). One clone from participant SCOPE2046 gave rise to 11 QVOA isolates (Supplemental Figure 2) and was resistant to aNAbs (IC_{50} ~100 µg/ml) from both timepoints tested, after 4.5 and 25.3 years on ART (Figure 5F). The integration site was chr4: 451609(+), within the ZNF721 gene. ZNF genes have been associated with regions of heterochromatin, leading possibly to deeper proviral latency (95, 96). Large clones integrated into ZNF721 have been previously detected in PWH on ART and elite controllers, in some cases with viral outgrowth assays (93, 97–100). Duplex ddPCR analysis on five cell samples spanning 11 years of ART showed that the frequency of this clone was stable (average 6.4/million resting $CD4^+$ T cells;

Figure 7, B and C). This was 1.1-2.5% of the average frequency of all proviruses assayed (347/million resting $CD4^+$ T cells, determined as ½ of the LTR frequency). For perspective, ~90% of proviruses are defective in PWH on ART (101). The average frequency of intact proviruses in this participant was 9.5 copies/million resting $CD4^+$ T cells, as determined by the IPDA (102), using the same cell samples. Thus, on average, this stable resistant outgrowth clone makes up 67% of all intact proviruses, consistent with the highly aNAb-resistant reservoir in this donor (Figure 1B). The second integration site match was for the major outgrowth clone (23 isolates) from SCOPE2256 (Supplemental Figure 2). This clone showed aNAb resistance (IC_{50} >100 µg/ml) over 13 years of ART (Figure 5G). The integration site was chr19: 58193728(-), within the ZNF274 gene. Chromosome 19 is enriched with repressive chromatin marks covering ZNF genes (95, 103, 104). Proviral clones integrated in chromosome 19 (19, 98), including ZNF274 (105), have been identified in elite controllers and PWH on ART. In three samples spanning 6 years of ART, the frequency of this provirus remained stable (average 61.2/million resting $CD4^+$ T cells; Figure 7, B and C). The average frequency of total proviruses was 1835 copies/million resting $CD4^+$ T cells, and the average frequency of intact proviruses was 277.2/million resting $CD4^+$ T cells. Thus, this resistant outgrowth clone is a small fraction of all persistent proviruses (2.1-4.2%) but is a substantial proportion of the intact reservoir, on average nearly 25%. These data support long-term persistence of large aNAb-resistant outgrowth clones that are inducible in the QVOA despite integration into ZNF genes and are potentially capable of causing rebound due to aNAb resistance.

Discussion

aNAbs block outgrowth of a fraction of inducible, replication-competent reservoir viruses (30, 106). Here, we analyzed aNAb activity against outgrowth viruses from 31 PWH on ART. Substantial aNAb-resistance (IC_{50} of contemporaneous IgG: >100 μg/ml) was found in the majority of participants using multiple analyses: fraction of all distinct isolates, fraction of all isolates including members of a potential clone, and those parameters on a per person basis. For downstream analysis, these participants were split into groups with high or low aNAb resistance. Resistance to neutralization tended to correlate with longer times on uninterrupted ART.

Using a previously described pharmacodynamic metric for logs of inhibition produced by an antiviral agent (IIP, (80–82, 84)), we predicted the in vivo activity of aNAbs at physiologic IgG concentrations, which are much higher than antibody concentrations used in neutralization assays. This analysis revealed that many isolates are actually susceptible to neutralization, but with IIP values of 1-3 (1-3 logs of inhibition of single round infection at physiologic IgG concentrations). This is in the range observed for many single antiretroviral drugs (80, 82, 85), a level of inhibition that leads to rapid selection of resistance. Previous studies have shown that IIP values >5 are required to produce complete suppression of viral replication (80, 82, 85). This level of inhibition has been observed in a recent case of post-treatment control that appears to be mediated by aNAbs (107).

We found that only rare isolates were neutralized at this level. Importantly, although few replication-competent isolates are potently neutralized by aNAbs in in vitro neutralization assays, a lower degree of neutralizing activity may be sufficient to prevent viral rebound from individual latently infected cells once suppression of viral replication has been achieved.

A consistent feature of effective neutralization is a high slope or Hill coefficient, reflecting cooperativity in the action of the antibody (108). Previous studies of bNAbs showed that antibodies targeting different regions of the Env trimer have different slopes (83). The highest slope values of ~1.5 were observed for antibodies targeting the CD4 binding site and the V3 glycan epitopes. Regarding mechanism, some classes of antiretroviral drugs have cooperative dose-response curves even though the drugs target viral proteins that are univalent with respect to the inhibitor (108). This form of cooperativity is observed when infectivity is the readout and multiple copies of the targeted viral protein participate in the relevant step in the virus life cycle. For antibodies, additional factors may give rise to cooperative dose-response curves, including the bivalent nature of IgG, the trimeric nature of the Env spike, the possible requirement for multiple trimers to mediate fusion, and, for aNAbs, the cooperation between non-competing antibodies that bind distinct epitopes. For example, it is possible that binding of one IgG induces a conformational change that facilitates the binding of additional antibodies.

The observed resistance to aNAbs was not solely due to general waning of the antibody response. Antibodies from participants generally neutralized the tier 1 virus SF162 (86, 87). Although longitudinal samples spanning multiple decades were only available for three participants, we showed that for these three PWH, the ability to neutralize SF162 was maintained over 13-21 years of ART. Over the same time intervals, we observed waning, stability, and improvement of aNAb activity against autologous outgrowth viruses, depending on the participant. These results suggest that some aNAbs can persist over 20 years of suppressive ART. Other studies have shown that aNAb responses can mature and persist in the presence of ART (74, 109–112).

To investigate other mechanisms for increased aNAb resistance, we conducted in vitro ADCC assays with target cells expressing participant-derived *env* sequences. For three long-term ART participants, we found ADCC activity against cells expressing all of the relevant donor Envs, with a preference for killing of cells expressing aNAb-sensitive Envs. However, purified autologous IgG contains both neutralizing and non-neutralizing antibodies to Env at unknown proportions (89–92, 113). This makes it difficult to distinguish the degree of selection mediated by the two types of antibodies. Many antibodies to the Env protein are not neutralizing, binding instead to epitopes exposed on open Env trimers, monomeric gp120, or gp41 stumps (114). Non-neutralizing antibodies have been shown to have a protective effect, exerting partial control of viremia early during infection (115). Both types of antibodies can select for escape mutations (92, 116). Non-neutralizing antibodies appear within 2-4 weeks of infection (117). They can mediate multiple Fc-mediated effector functions, including the release of inflammatory mediators, phagocytosis, and ADCC (118). In the RV144 vaccine trial, the only human vaccine trial to demonstrate measurable efficacy, higher ADCC activity was associated with protection (119, 120). Yet, in the follow up trial HVTN702, no efficacy was demonstrated (121).

Our study has limitations. Because longitudinal samples spanning over two decades of suppressive ART are generally not available, we compared differences in aNAb activity cross-sectionally among PWH who had been on ART for different lengths of time. Nevertheless, the observed aNAb-resistance in PWH on very long-term ART was not dependent on the comparison cohort. Definitive conclusions regarding the mechanism of resistance will require longitudinal analysis of samples collected over multiple decades on ART. A complication with the ADCC assay is that these experiments used NK cells from uninfected donors, rather than matched donor cells. During HIV-1 infection, NK cells undergo progressive dysregulation (122), which may impact the efficiency of ADCC-mediated killing.

In summary, our analysis of autologous antibody function and persistence revealed a large proportion of isolates with resistance to neutralization in PWH on long-term ART. This was not exclusively due to the waning of the antibody response. For future antibody-based therapeutic approaches, it will be important to determine whether memory B cells capable of producing aNAbs can be restimulated. It is possible that the observed resistance also reflects a selection process that favors aNAb-resistant viruses. These results emphasize the importance of starting ART early to limit the size of the reservoir (123) and the evolution of aNAb-resistant escape variants.

Methods

Sex as a biological variable

Sex was not considered as a biological variable. Both sexes were represented, although most participants were male. Our findings are expected to be relevant to both sexes.

Study participants

Participants were selected based on clinical records of viral suppression on ART (4-27 years). Acutely treated PWH (ART initiation within 2 months of infection) were excluded. All participants maintained generally undetectable plasma HIV-1 RNA levels. Five exceptions were DEL-SPC-015, -017, and -019 who previously received VRC01 and an ATI in ACTG trial A5340 (54, 61), as well as DEL-SPC-012 and JH448 who had periods of non-adherence. Peripheral blood samples or deidentified leukapheresis samples were obtained from 4 participants in the UCSF SCOPE cohort, 5 participants at the University of Toronto, 9 participants at the University of Pennsylvania, and 13 participants from the Johns Hopkins Hospital Bartlett Clinic. Participant characteristics are shown in Supplemental Figure 1 and Supplemental Table 1.

Isolation of resting $CD4^{+}$ T cells and plasma

Peripheral blood mononuclear cells (PBMCs) and plasma were separated from blood and leukapheresis samples by Ficoll gradient centrifugation. Plasma was stored at -80°C. Total $CD4^{+}$ T cells were isolated using the EasySep™ Human $CD4^{+}$ T Cell Enrichment Kit (19052, STEMCELL Technologies). Resting $CD4^{+}$ T cells were isolated from $CD4^{+}$ T cells by negative selection via CD25 Microbeads II, CD69 MicroBead Kit II, and anti-HLA-DR Microbeads (130-092-983, 130-092-355, 130-046-101, Miltenyi Biotec).

Quantitative viral outgrowth assay (QVOA)

The QVOA was set up with purified resting $CD4^+$ T cells as previously described (15, 77, 78). After day 21, an HIV p24 ELISA assay (NEK050A001KT, Revvity) was carried out on culture supernatants. Infectious units per million (IUPM) resting $CD4^+$ T cells were determined using maximal-likelihood limiting-dilution statistics with IUPMStats v1.0 as previously described (124). $p24^+$ supernatants were stored at -80°C.

Viral RNA isolation, cDNA synthesis, and sequencing of env

Thawed $p24^+$ QVOA supernatants were spun at 5,000xg at 4°C for 15 minutes to remove cells and debris and then RNA was extracted using 96-well spin plates according to the manufacturer protocol (Zymo Research). Eluted RNA was reverse transcribed with SuperScript III Reverse Transcriptase (Invitrogen) using the envelope-specific primer env3out (5′-TTGCTACTTGTGATTGCTCCATGT-3′) (125) as previously described (15). The cDNA was used as a template for full-length *env* sequencing by nested inner and outer PCRs as described previously (125) with the modified primer env3in (5′-TTTGACCACTTGCCACCCAT-3′) (15). Input DNA was run at limiting dilution so that <30% wells were positive across 12 replicates after visualizing on 1% agarose gels. PCR products (~3kb) were then cleaned using the Monarch PCR and DNA Cleanup Kit (New England Biolabs) according to the manufacturer protocol and submitted for Sanger sequencing (Azenta) using the primers env5out (125), env3out (125), BKRev16 (22, 30), and BKFor16 (22, 30).

Isolation of autologous IgG

Plasma was heat-inactivated at 56°C for 40 minutes. Autologous IgG antibodies were purified using NAb™ Protein A Plus Spin Columns (Thermo Fisher Scientific) according to the manufacturer's protocol. Buffer was exchanged multiple times using Slide-A-Lyzer™ G3 Dialysis Cassettes, 10K MWCO (Thermo Fisher Scientific) in phosphate-buffered saline (PBS), pH 7.2, at 4°C. IgG was collected and sterile-filtered in 0.22 µM centrifugal filter tubes (Millipore). IgG concentrations were determined by absorbance at 280 nm on a microvolume UV-Vis spectrophotometer (Thermo Fisher).

HIV-1 western blot

Qualitative detection of HIV-1 antibodies was performed using the GS HIV-1 Western Blot Kit (32508, Bio-Rad) according to the manufacturer's protocol.

Single-round pseudovirus generation

For neutralization assays, full length HIV-1 *env* sequences were transferred into *env* expression vectors by TA cloning. Additional 3' A overhangs were first added by incubation with 0.2mM dNTPs (Thermo Fisher Scientific), 1x PCR Buffer providing 1.5 mM MgCl (Qiagen), and 1U Taq DNA Polymerase (Qiagen) in a 20 µl reaction for 20 minutes at 72°C. After purification with the Monarch PCR and DNA Cleanup Kit (New England Biolabs), the PCR products were cloned using the pcDNA 3.4 TOPO TA Cloning Kit (Thermo Fisher Scientific). Plasmids were screened by colony PCR using Quick-Load Taq 2X Master Mix (New England Biolabs) and Sanger sequencing (Azenta). Colonies with HIV-1 *env* in the correct orientation were purified by ZymoPURE II Plasmid Maxiprep Kit (Zymo Research). Then, 12.5 µg of the purified plasmid were cotransfected with 15 µg of pNL4-3-ΔEnv-GFP using Lipofectamine 3000 Transfection Reagent (Thermo Fisher Scientific) into HEK293T cells (ATCC) in the presence of 2.5 µg of pAdvantage (Promega) to enhance protein expression. The SF162 *env* was provided by Michael S. Seaman. Viral supernatants containing isolate-specific Env-expressing pseudoviruses were harvested 65 hours after transfection, centrifuged to remove debris, filtered with 0.45 µM centrifugal filter tubes (Millipore), snap frozen on dry ice, and stored at –80°C.

Neutralization assays

Pseudoviruses were titrated on TZM-bl cells (126, 127) (NIH AIDS Reagent Program) to determine the linear range for infection as described previously (127). HIV-1 Env pseudoviruses were added to serially diluted IgG and preincubated for 90 minutes at 37°C. Then, 10,000 TZM-bl cells were added with a final concentration of 50 µg/mL DEAE-dextran. Triplicate control wells were set up with cells only (no virus, no antibody) and cells with virus (no antibody). After 48 hours at 37°C, infection was measured by quantification of luciferase using the Bright-Glo Luciferase Assay System (Promega), according to manufacturer instructions, and luminescence detection on a Varioskan LUX Multimode Microplate Reader (Thermo Fisher Scientific). IgG dilutions that inhibited 50% of viral infection (IC_{50}) were determined as previously reported (80) using the linear portion of the median effect plot. The maximum degree of infection was determined from wells with no or low concentrations of IgG. bNAbs used in neutralization assays, VRC01 and 10-1074, were from NIH AIDS Reagent Program (ARP-12033, ARP-12477. PGDM1400 was provided by Dennis R. Burton.

Replication-competent reporter virus generation

For ADCC assays, participant *env* sequences were inserted into the replication-competent NL4-3-ΔNef-eGFP backbone by Gibson assembly. Participant *envs* were amplified with the forward primer: 5’-GAGCAGAAGACAGTGGCAATGA-3’ and reverse primer: 5’-gagcggccgcgccaccCATCTTATAGCAAAGCCCTTTCYAAGCC-3’ containing overhangs that match the vector backbone. PCR cycling was as follows: 98°C for 30 seconds, followed by 30 cycles of 98°C for 10 seconds, 60°C for 10 seconds, and 72°C for 2 minutes, and then a final extension of 72°C for 5 minutes. Next, the backbone was amplified with two reactions. The first amplification used the forward primer 5’-GATAATACCGCGCCACATAGCAGAAC-3’ and reverse primer 5’-CATTGCCACTGTCTTCTGCTCTTTC-3’. PCR cycling was as follows: 98°C for 30 seconds, followed by 30 cycles of 98°C for 10 seconds, 60°C for 10 seconds, and 72°C for 7 minutes, and then a final extension of 72°C for 7 minutes. The second amplification used the forward primer 5'-GATGGGTGGCGCGGC-3' and reverse primer 5'-CTGCTATGTGGCGCGGTATTATCC-3'. PCR cycling was as follows: 98°C for 30 seconds, followed by 30 cycles of 98°C for 10 seconds, 60°C for 10 seconds, and 72°C for 5 minutes, and then a final extension of 72°C for 7 minutes. PCR reactions were performed using 1 ng template, 1x Superfi II Buffer, 0.2 mM dNTPs, 0.25 uM forward and reverse primers, and 2U of Platinum SuperFi II DNA Polymerase (Thermo Fisher Scientific). Reactions were digested with DpnI (New England Biolabs) by incubation for 1 hour at 37°C to remove parental plasmid DNA templates and immediately cleaned by Monarch PCR and DNA Cleanup Kit (New England Biolabs). A DNA molar ratio for the insert:backbone1:backbone2 was 2:1:1. The combined DNA was mixed with 2 µL of 5X In-Fusion Snap Assembly Master Mix (Takara Bio) in a 10 µL reaction and incubated at 50°C for 15 minutes. Then, 2.5 µl of the Gibson assembly reaction were transformed in NEB Stable Competent E. coli (New England Biolabs) and grown on LB agar plates containing 100 µg/mL ampicillin for 16 hours at 30°C. Single colonies were selected and grown in LB broth for 16 hours at 30°C. Plasmid DNA was isolated using Zyppy Plasmid Miniprep Kit (Zymo Research) and submitted for Nanopore sequencing (Plasmidsaurus). Then, 27.5 µg of the plasmid and 2.5 µg of pAdvantage (Promega) were transfected into HEK293T cells (ATCC) using Lipofectamine 3000 Transfection Reagent (Thermo Fisher Scientific). Supernatants were harvested 65 hours after transfection, centrifuged to remove debris, filtered with 0.45 µM centrifugal filter tubes (Millipore), concentrated with Lenti-X Concentrator (Takara Bio), and stored at –80°C.

ADCC assay

Replication-competent reporter viruses were titrated to determine the amount needed to achieve ~20-30% infection of target CEM.NKR.CCR5 cells (88) (NIH HIV Reagent Program), as assessed by GFP expression. At least 20,000 target cells/condition at 10^6 cells/ml were spinoculated with concentrated reported viruses at 1200xg for 2 hours at 30°C. Following infection, CEM.NKR.CCR5 cells were washed and cultured for 2 days at 37°C. Uninfected donor NK cells were isolated from leukopaks (New York Blood Center) by negative selection (STEMCELL Technologies) and cultured overnight with 50 U/ml recombinant human IL-2 to maintain viability. Before co-culture, infected CEM.NKR.CCR5 cells were stained with 0.5 µM CellTrace Violet (CTV, C34571 Thermo Fisher Scientific). Then, NK cells and stained infected CEM.NKR.CCR5 cells were co-cultured at an effector:target ratio of 9:1 with serial dilutions of purified participant IgG and 50 U/ml IL-2 to enhance killing. Antiretroviral drugs (5 µM tenofovir disoproxil fumarate and 5 µM emtricitabine) were added to prevent new cycles of infection. After 4 hours at 37°C, cells were washed in PBS, stained with LIVE/DEAD Fixable Near-IR Dead Cell Stain Kit (1:1000 dilution, L34975 Thermo Fisher Scientific), and washed. Samples were run on an Intellicyt iQue Screener Plus. As shown in Supplemental Figure 8, data were analyzed with FlowJo by gating on the target cells (CTV+) and then live infected cells (live GFP+).

Intact proviral DNA assay

Genomic DNA was extracted (QIAamp DNA Mini Kit, Qiagen) from each participant's resting $CD4^+$ T cells and used in the IPDA as previously described (102).

Integration site analysis

Following unbiased whole genome amplification, limiting-diluted HIV-1 DNA from each well was split and separately subjected to viral sequencing and integration site analysis in MIP-Seq analysis, as described previously (93). Integration sites were obtained using integration site loop amplification (ISLA) (20).

Duplex LTR and integration site quantification by ddPCR

Custom ddPCR assays to quantify proviruses with ZNF721 and ZNF274 integration sites were designed based on the host-U3 junction, with the fluorescently labeled probe positioned across the integration site (28). For ZNF721, the forward primer 5'-TACCCTTTCTCCCTTCTCCA-3', reverse primer 5'-GTTCTGCCAATCAGGGAAGTA, and probe 5'HEX/TTCCCACTT/ZEN/GGAAGGGCTAGTTTAC/3'IABkFQ were used. For ZNF274, the forward primer 5'-GCACTGCATCTGGCTTATTATTT-3', reverse primer 5'-CAATCAGGGAAGTAGCCTTGT-3', and probe 5'HEX/TGTCAGGTG/ZEN/GTCTTTGGAAGGGATAATATAC/3'IABkFQ were used. For duplex quantification of all LTRs (R-U5) (94), the forward primer 5'-CTTAAGCCTCAATAAAGCTTGCC-3', reverse primer 5'-GGATCTCTAGTTACCAGAGTC-3', and probe 5'FAM/AGTAGTGTG/ZEN/TGCCCGTCTG/3'IABkFQ were incorporated into the ZNF reaction mix. Primers and probes had a final concentration of 900 nM and 250 nM, respectively. Reaction mixes contained ddPCR Supermix for probes (no dUTPs) (Bio-Rad). Parallel quantification of RPP30 was performed as described (102) to normalize for shearing and calculate cell equivalents. Genomic DNA extracted (QIAamp DNA Mini Kit, Qiagen) from resting $CD4^+$ T cells was added to reactions so that droplets contained no more than one provirus. Droplets were made on the Bio-Rad Automated Droplet Generator. PCR reactions were run with the following parameters: 95°C for 10 minutes, 95°C for 30 seconds, 56°C for 2 minutes (steps 2 to 3 for 49 cycles), 98°C for 10 minutes, hold at 4°C (temperature change rate 2°C/second). Droplets were read on Bio-Rad QX200 Droplet Reader and analyzed using QuantaSoft. Frequencies of LTR and integration sites were based on shearing and cell equivalent input of RPP30.

Sequence alignment and phylogenetic analysis

After Sanger sequencing of *env*, contigs were assembled and checked for quality in Geneious. BioEdit was used to align sequences to HXB2 and remove defective *envs*. To identify distinct sequences, we used ElimDupes (https://www.hiv.lanl.gov/content/sequence/elimdupesv2/elimdupes.html). Maximum-likelihood phylogenetic trees were generated with PHYML 3.0 (http://www.atgc-montpellier.fr/phyml/) as previously described (30) and with bootstrapping of 100 replicates. MEGA11 (https://www.megasoftware.net/) was used to visualize the generated tree. Tree annotations were made in Adobe Illustrator.

Statistics

Statistical significance was calculated with normality tests, Mann-Whitney tests, Friedman test followed by Dunn's test for multiple comparisons, and Spearman's rank correlation using GraphPad Prism 10.4. A P value of 0.05 was considered significant.

Study approval

The Institutional Review Boards of the University of Pennsylvania (Philadelphia FIGHT), UCSF (SCOPE, Human Research Protection Program), Johns Hopkins University Bartlett Clinic, and University of Toronto (Unity Health Toronto) approved the study. All participants provided written informed consent.

Data availability

All HIV-1 sequences are available in the NCBI's GenBank (accession numbers PV352008 - PV352146). Data for the figures are in the Supporting Data Values file.

Author Contributions

NFM, JV, HW, and MM conducted experiments. VH designed the Gibson assembly method for replication-competent reporter viruses. TSN, XY, and ML performed integration site analysis. NFM, MM, and FRS optimized and designed custom duplex ddPCR assay in Figure 7. JL, AS, KL, KM, PT, LJM, CK, RH, and SD enrolled participants and provided participant samples with clinical histories. NFM, JV, MM, JMS, and RFS investigated the results. NFM, JMS, and RFS wrote the manuscript with feedback from all authors.

Acknowledgements

Thank you to study participants. Figure 6A was created with BioRender. This work was supported by NIH Martin Delaney Collaboratories for HIV Cure Research grant awards UM1AI164556, UM1AI164570, and UM1AI164560, and the Howard Hughes Medical Institute. We thank Ola Mohamed, Matthew Fair, and Jessicamarie Morris for assistance with patient-based studies. This study was also supported by the Robert I. Jacobs Fund of the Philadelphia Foundation (LM) and a Herbert Kean, M.D., Family Professorship (LM).

References

1. Chun TW, et al. In vivo fate of HIV-1-infected T cells: quantitative analysis of the transition to stable latency. *Nat Med*. 1995;1(12):1284–1290.

2. Chun TW, et al. Quantification of latent tissue reservoirs and total body viral load in HIV-1 infection. *Nature*. 1997;387(6629):183–188.

3. Finzi D, et al. Identification of a Reservoir for HIV-1 in Patients on Highly Active Antiretroviral Therapy. *Science (1979)*. 1997;278(5341):1295–1300.

4. Wong JK, et al. Recovery of Replication-Competent HIV Despite Prolonged Suppression of Plasma Viremia. *Science (1979)*. 1997;278(5341):1291–1295.

5. Chun TW, et al. Presence of an inducible HIV-1 latent reservoir during highly active antiretroviral therapy. *Proc Natl Acad Sci U S A*. 1997;94(24):13193–13197.

6. Hammer SM, et al. A controlled trial of two nucleoside analogues plus indinavir in persons with human immunodeficiency virus infection and CD4 cell counts of 200 per cubic millimeter or less. *N Engl J Med*. 1997;337(11):725–733.

7. Gulick RM, et al. Treatment with indinavir, zidovudine, and lamivudine in adults with human immunodeficiency virus infection and prior antiretroviral therapy. *N Engl J Med*. 1997;337(11):734–739.

8. Perelson AS, et al. Decay characteristics of HIV-1-infected compartments during combination therapy. *Nature*. 1997;387(6629):188–191.

9. Davey RT, et al. HIV-1 and T cell dynamics after interruption of highly active antiretroviral therapy (HAART) in patients with a history of sustained viral suppression. *Proc Natl Acad Sci U S A*. 1999;96(26):15109–15114.

10. Rothenberger MK, et al. Large number of rebounding/founder HIV variants emerge from multifocal infection in lymphatic tissues after treatment interruption. *Proc Natl Acad Sci U S A*. 2015;112(10):E1126–E1134.

11. Colby DJ, et al. Rapid HIV RNA rebound after antiretroviral treatment interruption in persons durably suppressed in Fiebig I acute HIV infection. *Nat Med*. 2018;24(7):923–926.

12. Finzi D, et al. Latent infection of CD4+ T cells provides a mechanism for lifelong persistence of HIV-1, even in patients on effective combination therapy. *Nature Medicine 1999 5:5*. 1999;5(5):512–517.

13. Siliciano JD, et al. Long-term follow-up studies confirm the stability of the latent reservoir for HIV-1 in resting CD4+ T cells. *Nat Med*. 2003;9(6):727–728.

14. Crooks AM, et al. Editor's choice: Precise Quantitation of the Latent HIV-1 Reservoir: Implications for Eradication Strategies. *J Infect Dis*. 2015;212(9):1361.

15. McMyn NF, et al. The latent reservoir of inducible, infectious HIV-1 does not decrease despite decades of antiretroviral therapy. *J Clin Invest*. 2023;133(17).

16. Tobin NH, et al. Evidence that low-level viremias during effective highly active antiretroviral therapy result from two processes: expression of archival virus and replication of virus. *J Virol*. 2005;79(15):9625–9634.

17. Bailey JR, et al. Residual human immunodeficiency virus type 1 viremia in some patients on antiretroviral therapy is dominated by a small number of invariant clones rarely found in circulating CD4+ T cells. *J Virol*. 2006;80(13):6441–6457.

18. Wagner TA, et al. An increasing proportion of monotypic HIV-1 DNA sequences during antiretroviral treatment suggests proliferation of HIV-infected cells. *J Virol*. 2013;87(3):1770–1778.

19. Maldarelli F, et al. HIV latency. Specific HIV integration sites are linked to clonal expansion and persistence of infected cells. *Science*. 2014;345(6193):179–183.

20. Wagner TA, et al. HIV latency. Proliferation of cells with HIV integrated into cancer genes contributes to persistent infection. *Science*. 2014;345(6196):570–573.

21. Lorenzi JCC, et al. Paired quantitative and qualitative assessment of the replication-competent HIV-1 reservoir and comparison with integrated proviral DNA. *Proc Natl Acad Sci U S A*. 2016;113(49):E7908–E7916.

22. Bui JK, et al. Proviruses with identical sequences comprise a large fraction of the replication-competent HIV reservoir. *PLoS Pathog*. 2017;13(3).

23. Hosmane NN, et al. Proliferation of latently infected CD4 + T cells carrying replication-competent HIV-1: Potential role in latent reservoir dynamics. *J Exp Med*. 2017;214(4):959–972.

24. Reeves DB, et al. A majority of HIV persistence during antiretroviral therapy is due to infected cell proliferation. *Nat Commun*. 2018;9(1):1–16.

25. Henrich TJ, et al. Human Immunodeficiency Virus Type 1 Persistence Following Systemic Chemotherapy for Malignancy. *J Infect Dis*. 2017;216(2):254–262.

26. Mendoza P, et al. Antigen-responsive CD4+ T cell clones contribute to the HIV-1 latent reservoir. *J Exp Med*. 2020;217(7).

27. Gantner P, et al. Single-cell TCR sequencing reveals phenotypically diverse clonally expanded cells harboring inducible HIV proviruses during ART. *Nat Commun*. 2020;11(1).

28. Simonetti FR, et al. Antigen-driven clonal selection shapes the persistence of HIV-1–infected CD4+ T cells in vivo. *J Clin Invest*. 2021;131(3).

29. Moskovljevic M, et al. Cognate antigen engagement induces HIV-1 expression in latently infected CD4+ T cells from people on long-term antiretroviral therapy. *Immunity*. 2024;57(12):2928-2944.e6.

30. Bertagnolli LN, et al. Autologous IgG antibodies block outgrowth of a substantial but variable fraction of viruses in the latent reservoir for HIV-1. *Proc Natl Acad Sci U S A*. 2020;117(50):32006–32077.

31. Burton DR, Mascola JR. Antibody responses to envelope glycoproteins in HIV-1 infection. *Nat Immunol*. 2015;16(6).

32. Kumar S, et al. An Overview of Human Anti-HIV-1 Neutralizing Antibodies against Diverse Epitopes of HIV-1. *ACS Omega*. 2023;8(8).

33. Burton DR. Antiviral neutralizing antibodies: from in vitro to in vivo activity. *Nature Reviews Immunology 2023 23:11*. 2023;23(11):720–734.

34. Doores KJ, et al. Envelope glycans of immunodeficiency virions are almost entirely oligomannose antigens. *Proc Natl Acad Sci U S A*. 2010;107(31).

35. Moscoso CG, et al. Trimeric HIV Env provides epitope occlusion mediated by hypervariable loops. *Sci Rep*. 2014;4.

36. Kwong PD, et al. HIV-1 evades antibody-mediated neutralization through conformational masking of receptor-binding sites. *Nature*. 2002;420(6916).

37. Mansky LM, Temin HM. Lower in vivo mutation rate of human immunodeficiency virus type 1 than that predicted from the fidelity of purified reverse transcriptase. *J Virol*. 1995;69(8).

38. Wei X, et al. Viral dynamics in human immunodeficiency virus type 1 infection. *Nature*. 1995;373(6510).

39. Ho DD, et al. Rapid turnover of plasma virions and CD4 lymphocytes in HIV-1 infection. *Nature*. 1995;373(6510).

40. Albert J, et al. Rapid development of isolate-specific neutralizing antibodies after primary HIV-1 infection and consequent emergence of virus variants which resist neutralization by autologous sera. *AIDS*. 1990;4(2).

41. Richman DD, et al. Rapid evolution of the neutralizing antibody response to HIV type 1 infection. *Proc Natl Acad Sci U S A*. 2003;100(7).

42. Wei X, et al. Antibody neutralization and escape by HIV-1. *Nature*. 2003;422(6929).

43. Tomaras GD, Haynes BF. HIV-1-specific antibody responses during acute and chronic HIV-1 infection. *Curr Opin HIV AIDS*. 2009;4(5).

44. Moore PL, et al. Virological features associated with the development of broadly neutralizing antibodies to HIV-1. *Trends Microbiol*. 2015;23(4).

45. Burton DR, Hangartner L. Broadly Neutralizing Antibodies to HIV and Their Role in Vaccine Design. *Annu Rev Immunol*. 2016;34.

46. Haynes BF, et al. Strategies for HIV-1 vaccines that induce broadly neutralizing antibodies. *Nat Rev Immunol*. 2023;23(3).

47. Mikell I, et al. Characteristics of the earliest cross-neutralizing antibody response to HIV-1. *PLoS Pathog*. 2011;7(1).

48. Euler Z, Schuitemaker H. Cross-reactive broadly neutralizing antibodies: timing is everything. *Front Immunol*. 2012;3:215.

49. Simek MD, et al. Human Immunodeficiency Virus Type 1 Elite Neutralizers: Individuals with Broad and Potent Neutralizing Activity Identified by Using a High-Throughput Neutralization Assay together with an Analytical Selection Algorithm. *J Virol*. 2009;83(14).

50. Tomaras GD, et al. Polyclonal B Cell Responses to Conserved Neutralization Epitopes in a Subset of HIV-1-Infected Individuals. *J Virol*. 2011;85(21).

51. Kwong PD, Mascola JR. Human Antibodies that Neutralize HIV-1: Identification, Structures, and B Cell Ontogenies. *Immunity*. 2012;37(3).

52. Hraber P, et al. Prevalence of broadly neutralizing antibody responses during chronic HIV-1 infection. *AIDS*. 2014;28(2).

53. Scheid JF, et al. HIV-1 antibody 3BNC117 suppresses viral rebound in humans during treatment interruption. *Nature*. 2016;535(7613).

54. Bar KJ, et al. Effect of HIV Antibody VRC01 on Viral Rebound after Treatment Interruption. *New England Journal of Medicine*. 2016;375(21).

55. Gaebler C, et al. Prolonged viral suppression with anti-HIV-1 antibody therapy. *Nature*. 2022;606(7913).

56. Sneller MC, et al. Combination anti-HIV antibodies provide sustained virological suppression. *Nature*. 2022;606(7913).

57. Julg B, et al. Safety and antiviral effect of a triple combination of HIV-1 broadly neutralizing antibodies: a phase 1/2a trial. *Nat Med*. 2024;30(12):3534–3543.

58. Bruel T, et al. Elimination of HIV-1-infected cells by broadly neutralizing antibodies. *Nat Commun*. 2016;7.

59. Ren Y, et al. Relationships between Neutralization, Binding, and ADCC of Broadly Neutralizing Antibodies against Reservoir HIV. *J Virol*. 2020;95(2).

60. Tuyishime M, et al. Improved killing of HIV-infected cells using three neutralizing and non-neutralizing antibodies. *Journal of Clinical Investigation*. 2020;130(10).

61. Salantes DB, et al. HIV-1 latent reservoir size and diversity are stable following brief treatment interruption. *J Clin Invest*. 2018;128(7):3102–3115.

62. Cohen YZ, et al. Relationship between latent and rebound viruses in a clinical trial of anti-HIV-1 antibody 3BNC117. *J Exp Med*. 2018;215(9):2311–2324.

63. Peluso MJ, et al. Differential decay of intact and defective proviral DNA in HIV-1–infected individuals on suppressive antiretroviral therapy. *JCI Insight*. 2020;5(4).

64. White JA, et al. Complex decay dynamics of HIV virions, intact and defective proviruses, and 2LTR circles following initiation of antiretroviral therapy. *Proc Natl Acad Sci U S A*. 2022;119(6):e2120326119.

65. Schröder ARW, et al. HIV-1 Integration in the Human Genome Favors Active Genes and Local Hotspots. *Cell*. 2002;110(4):521–529.

66. Han Y, et al. Resting CD4+ T Cells from Human Immunodeficiency Virus Type 1 (HIV-1)-Infected Individuals Carry Integrated HIV-1 Genomes within Actively Transcribed Host Genes. *J Virol*. 2004;78(12):6122.

67. Sun W, et al. Footprints of innate immune activity during HIV-1 reservoir cell evolution in early-treated infection. *Journal of Experimental Medicine*. 2024;221(11).

68. Xiaodong Lian A, et al. Progressive transformation of the HIV-1 reservoir cell profile over two decades of antiviral therapy. *Cell Host Microbe*. 2022;31(1):83–96.

69. Jiang C, et al. Distinct viral reservoirs in individuals with spontaneous control of HIV-1. *Nature*. 2020;585(7824):261–267.

70. Hua S, et al. Pegylated Interferon-α-Induced Natural Killer Cell Activation Is Associated with Human Immunodeficiency Virus-1 DNA Decline in Antiretroviral Therapy-Treated HIV-1/Hepatitis C Virus-Coinfected Patients. *Clinical Infectious Diseases*. 2018;66(12).

71. Hartana CA, et al. Immune correlates of HIV-1 reservoir cell decline in early-treated infants. *Cell Rep*. 2022;40(3).

72. Armani-Tourret M, et al. Selection of epigenetically privileged HIV-1 proviruses during treatment with panobinostat and interferon-α2a. *Cell*. 2024;187(5).

73. Wang FX, et al. Emergence of autologous neutralization-resistant variants from preexisting human immunodeficiency virus (HIV) quasi species during virus rebound in HIV type 1-infected patients undergoing highly active antiretroviral therapy. *Journal of Infectious Diseases*. 2002;185(5).

74. Esmaeilzadeh E, et al. Autologous neutralizing antibodies increase with early antiretroviral therapy and shape HIV rebound after treatment interruption. *Sci Transl Med*. 2023;15(695).

75. Nettles RE, et al. Intermittent HIV-1 viremia (Blips) and drug resistance in patients receiving HAART. *JAMA*. 2005;293(7):817–829.

76. Maldarelli F, et al. ART suppresses plasma HIV-1 RNA to a stable set point predicted by pretherapy viremia. *PLoS Pathog*. 2007;3(4):484–488.

77. Siliciano JD, Siliciano RF. Enhanced culture assay for detection and quantitation of latently infected, resting CD4+ T-cells carrying replication-competent virus in HIV-1-infected individuals. *Methods Mol Biol*. 2005;304:3–15.

78. Laird GM, et al. Measuring the frequency of latent HIV-1 in resting CD4+ T cells using a limiting dilution coculture assay. *Methods in Molecular Biology*. 2016;1354:239–253.

79. Jorge Sepulveda. Reference Intervals and Laboratory Values. In: Goldman L, Cooney KA eds. *Goldman-Cecil Medicine*. Philadelphia: Elsevier Inc.; 2024:e1–e11

80. Shen L, et al. Dose-response curve slope sets class-specific limits on inhibitory potential of anti-HIV drugs. *Nat Med*. 2008;14(7).

81. Shen L, Siliciano RF. Viral reservoirs, residual viremia, and the potential of highly active antiretroviral therapy to eradicate HIV infection. *Journal of Allergy and Clinical Immunology*. 2008;122(1).

82. Shen L, et al. A novel method for determining the inhibitory potential of anti-HIV drugs. *Trends Pharmacol Sci*. 2009;30(12).

83. Chou TC, Talalay P. Quantitative analysis of dose-effect relationships: the combined effects of multiple drugs or enzyme inhibitors. *Adv Enzyme Regul*. 1984;22(C).

84. Webb NE, et al. Dose-response curve slope helps predict therapeutic potency and breadth of HIV broadly neutralizing antibodies. *Nat Commun*. 2015;6.

85. Jilek BL, et al. A quantitative basis for antiretroviral therapy for HIV-1 infection. *Nat Med*. 2012;18(3).

86. Stamatatos L, et al. Effect of major deletions in the V1 and V2 loops of a macrophage-tropic HIV type 1 isolate on viral envelope structure, cell entry, and replication. *AIDS Res Hum Retroviruses*. 1998;14(13).

87. Seaman MS, et al. Tiered Categorization of a Diverse Panel of HIV-1 Env Pseudoviruses for Assessment of Neutralizing Antibodies. *J Virol*. 2010;84(3).

88. Trkola A, et al. A Cell Line-Based Neutralization Assay for Primary Human Immunodeficiency Virus Type 1 Isolates That Use either the CCR5 or the CXCR4 Coreceptor. *J Virol*. 1999;73(11).

89. Richard J, et al. CD4 mimetics sensitize HIV-1-infected cells to ADCC. *Proc Natl Acad Sci U S A*. 2015;112(20).

90. Mayr LM, et al. Non-neutralizing Antibodies Targeting the V1V2 Domain of HIV Exhibit Strong Antibody-Dependent Cell-mediated Cytotoxic Activity. *Sci Rep*. 2017;7(1).

91. Horwitz JA, et al. Non-neutralizing Antibodies Alter the Course of HIV-1 Infection In Vivo. *Cell*. 2017;170(4).

92. Mielke D, et al. ADCC-mediating non-neutralizing antibodies can exert immune pressure in early HIV-1 infection. *PLoS Pathog*. 2021;17(11).

93. Einkauf KB, et al. Intact HIV-1 proviruses accumulate at distinct chromosomal positions during prolonged antiretroviral therapy. *J Clin Invest*. 2019;129(3):988.

94. Anderson EM, Maldarelli F. Quantification of HIV DNA Using Droplet Digital PCR Techniques. *Curr Protoc Microbiol*. 2018;51(1).

95. Vogel MJ, et al. Human heterochromatin proteins form large domains containing KRAB-ZNF genes. *Genome Res*. 2006;16(12).

96. Seczynska M, Lehner PJ. The sound of silence: mechanisms and implications of HUSH complex function. *Trends in Genetics*. 2023;39(4).

97. Halvas EK, et al. HIV-1 viremia not suppressible by antiretroviral therapy can originate from large T cell clones producing infectious virus. *J Clin Invest*. 2020;130(11):5847–5857.

98. Jiang C, et al. A unique viral reservoir landscape in HIV-1 elite controllers. *Nature*. 2020;585(7824).

99. Huang AS, et al. Integration features of intact latent HIV-1 in CD4+ T cell clones contribute to viral persistence. *J Exp Med*. 2021;218(12).

100. Dragoni F, et al. Proviral location affects cognate peptide–induced virus production and immune recognition of HIV-1–infected T cell clones. *Journal of Clinical Investigation*. 2023;133(21).

101. Ho YC, et al. Replication-competent non-induced proviruses in the latent reservoir increase barrier to HIV-1 cure. *Cell*. 2013;155(3):540.

102. Bruner KM, et al. A novel quantitative approach for measuring the reservoir of latent HIV-1 proviruses. *Nature*. 2019;566(7742):120.

103. Lukic S, et al. The diversity of zinc-finger genes on human chromosome 19 provides an evolutionary mechanism for defense against inherited endogenous retroviruses. *Cell Death Differ*. 2014;21(3).

104. Begnis M, et al. Clusters of lineage-specific genes are anchored by ZNF274 in repressive perinucleolar compartments. *Sci Adv*. 2024;10(37):eado1662.

105. Cole B, et al. Extensive characterization of HIV-1 reservoirs reveals links to plasma viremia before and during analytical treatment interruption. *Cell Rep*. 2022;39(4).

106. Wilson A, et al. Characterizing the Relationship Between Neutralization Sensitivity and env Gene Diversity During ART Suppression. *Front Immunol*. 2021;12.

107. Zhuo J, et al. Autologous IgGs Mediate Log Reductions in HIV Infection in a PTC, Contributing to ART-Free Remission. In: *Poster 1344*. CROI Foundation/IAS-USA; 2025:

108. Shen L, et al. A critical subset model provides a conceptual basis for the high antiviral activity of major HIV drugs. *Sci Transl Med*. 2011;3(91).

109. Cohen MS, et al. Acute HIV-1 Infection. *New England Journal of Medicine*. 2011;364(20).

110. Mitchell JL, et al. Anti-HIV antibody development up to 1 year after antiretroviral therapy initiation in acute HIV infection. *Journal of Clinical Investigation*. 2022;132(1).

111. Schommers P, et al. Dynamics and durability of HIV-1 neutralization are determined by viral replication. *Nat Med*. 2023;29(11).

112. Whitehill GD, et al. Autologous neutralizing antibody responses after antiretroviral therapy in acute and early HIV-1. *J Clin Invest*. 2024;134(11).

113. von Bredow B, et al. Comparison of Antibody-Dependent Cell-Mediated Cytotoxicity and Virus Neutralization by HIV-1 Env-Specific Monoclonal Antibodies. *J Virol*. 2016;90(13).

114. Moore PL, et al. Nature of Nonfunctional Envelope Proteins on the Surface of Human Immunodeficiency Virus Type 1. *J Virol*. 2006;80(5).

115. Forthal DN, Finzi A. Antibody-dependent cellular cytotoxicity in HIV infection. *AIDS*. 2018;32(17).

116. Chung AW, et al. Immune escape from HIV-specific antibody-dependent cellular cytotoxicity (ADCC) pressure. *Proc Natl Acad Sci U S A*. 2011;108(18).

117. Tomaras GD, et al. Initial B-Cell Responses to Transmitted Human Immunodeficiency Virus Type 1: Virion-Binding Immunoglobulin M (IgM) and IgG Antibodies Followed by Plasma Anti-gp41 Antibodies with Ineffective Control of Initial Viremia. *J Virol*. 2008;82(24).

118. Nimmerjahn F, Ravetch J V. Fcγ receptors as regulators of immune responses. *Nat Rev Immunol*. 2008;8(1).

119. Haynes BF, et al. Immune-Correlates Analysis of an HIV-1 Vaccine Efficacy Trial. *New England Journal of Medicine*. 2012;366(14).

120. Yates NL, et al. Vaccine-induced Env V1-V2 IgG3 correlates with lower HIV-1 infection risk and declines soon after vaccination. *Sci Transl Med*. 2014;6(228).

121. Gray GE, et al. Vaccine Efficacy of ALVAC-HIV and Bivalent Subtype C gp120–MF59 in Adults. *New England Journal of Medicine*. 2021;384(12).

122. Moreno-Cubero E, et al. IL-15 reprogramming compensates for NK cell mitochondrial dysfunction in HIV-1 infection. *JCI Insight*. 2024;9(4).

123. Coffin JM, et al. Clones of infected cells arise early in HIV-infected individuals. *JCI Insight*. 2019;4(12).

124. Rosenbloom DIS, et al. Designing and Interpreting Limiting Dilution Assays: General Principles and Applications to the Latent Reservoir for Human Immunodeficiency Virus-1. *Open Forum Infect Dis*. 2015;2(4).

125. Evering TH, et al. Absence of HIV-1 Evolution in the Gut-Associated Lymphoid Tissue from Patients on Combination Antiviral Therapy Initiated during Primary Infection. *PLoS Pathog*. 2012;8(2).

126. Montefiori DC. Measuring HIV neutralization in a luciferase reporter gene assay. *Methods in Molecular Biology*. 2009;485.

127. Sarzotti-Kelsoe M, et al. Optimization and validation of the TZM-bl assay for standardized assessments of neutralizing antibodies against HIV-1. *J Immunol Methods*. 2014;409.

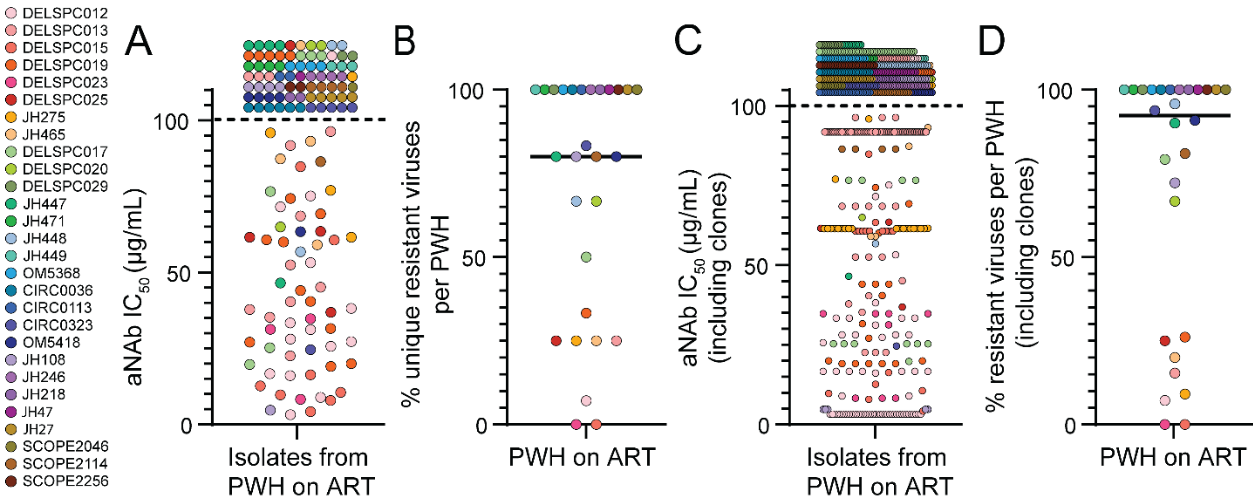

Figure 1. Variation in sensitivity of reservoir isolates to aNAbs. (**A**) aNAb IC_{50} values were determined in TZM.bl-based neutralization assays for distinct pseudoviruses generated from outgrowth viruses from PWH on ART (n = 138 isolates). Autologous IgG concentrations up to 100 µg/ml were used. Circles represent distinct isolates, and colors represent participants. (**B**) Percentage of distinct outgrowth viruses resistant (IC_{50} >100 µg/ml) to neutralization by contemporaneous aNAbs per PWH. Each data point (n = 28) represents the % of resistant viruses among the total number of viruses tested in each PWH. Bar represents median. (**C**) aNAb neutralization of distinct isolates shown in (A) with additional data points representing independent isolates from the same PWH with *env* sequences identical to those shown in (A), n = 591. IC_{50} values determined for one member of a set of isolates with identical *env* sequence were used for all members of the set. (**D**) Percentage of outgrowth viruses resistant to neutralization (IC_{50} >100 µg/ml) by aNAbs per PWH, n = 28, using values from (C). All isolates from each participant, including sequence-identical isolates, are considered in the percentage calculation. Bar represents median.

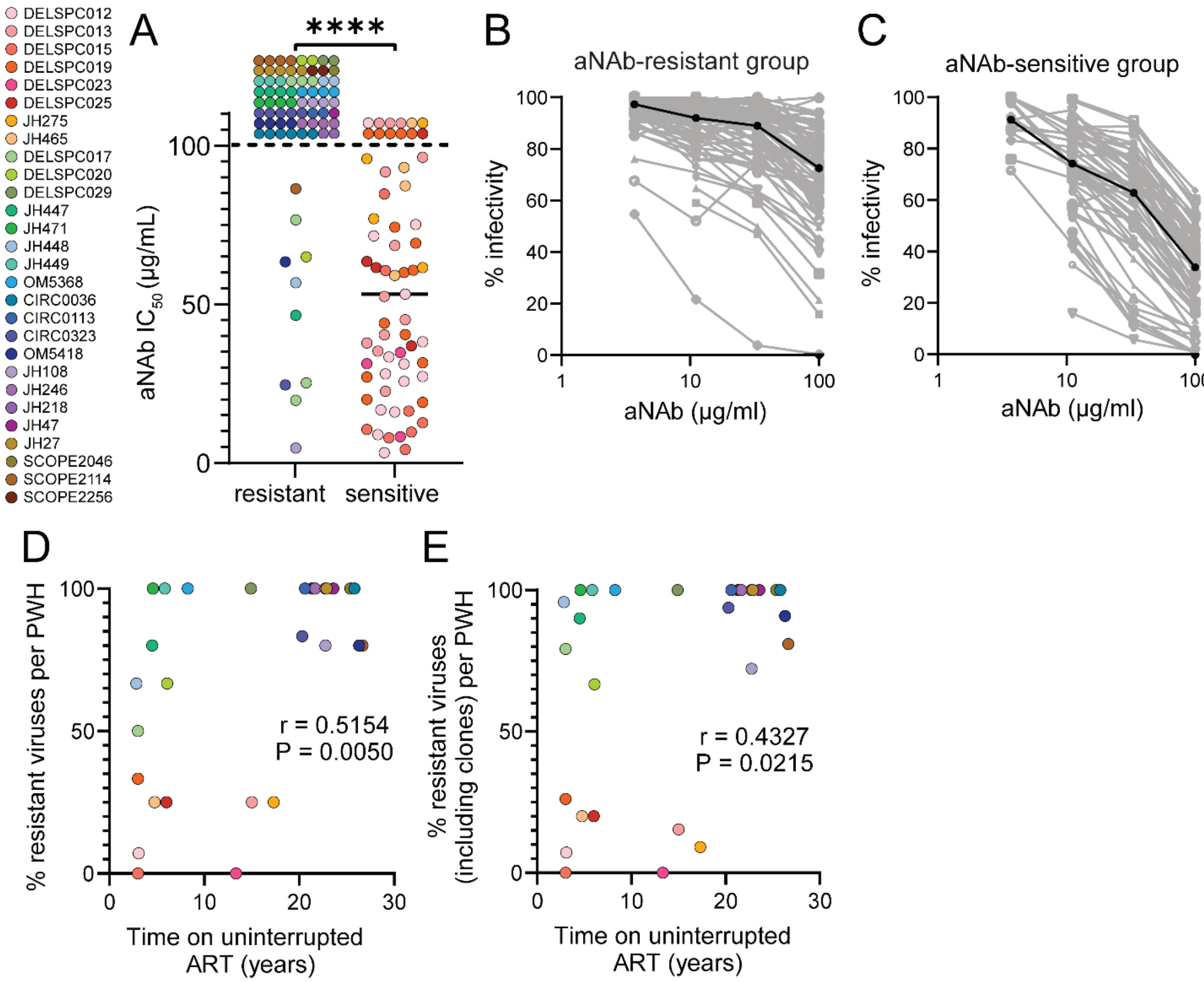

Figure 2. Understanding individual variation in aNAb resistance. PWH on ART were divided into two groups, those with aNAb-resistant or aNAb-sensitive reservoirs, based on Figure 1D. The aNAb-resistant group had ≥67% resistant isolates while the aNAb-sensitive group had ≤26% resistant isolates. (**A**) aNAb IC_{50} values for distinct pseudoviruses for the aNAb-resistant (n = 74 isolates) and aNAb-sensitive groups (n = 64 isolates). Circles represent distinct isolates, and colors represent participants. The Mann-Whitney test was used to calculate significance. **** = P < 0.0001. Bar represents median. (**B, C**) Dose-response curves for the inhibition of pseudovirus infectivity by autologous IgG for isolates from the aNAb-resistant (**B**, n = 74 isolates) and aNAb-sensitive (**C**, n = 64 isolates) groups. The median curve is overlayed in black. Data are reported as a mean % of maximum infectivity from triplicate measurements. (**D**) Percentage of resistant viruses per PWH from Figure 1B correlates with time on uninterrupted ART (Spearman's correlation, n = 28). (**E**) Percentage of resistant viruses per PWH, including sets of identical sequences from Figure 1D, correlates with time on uninterrupted ART (Spearman's correlation, n = 28).

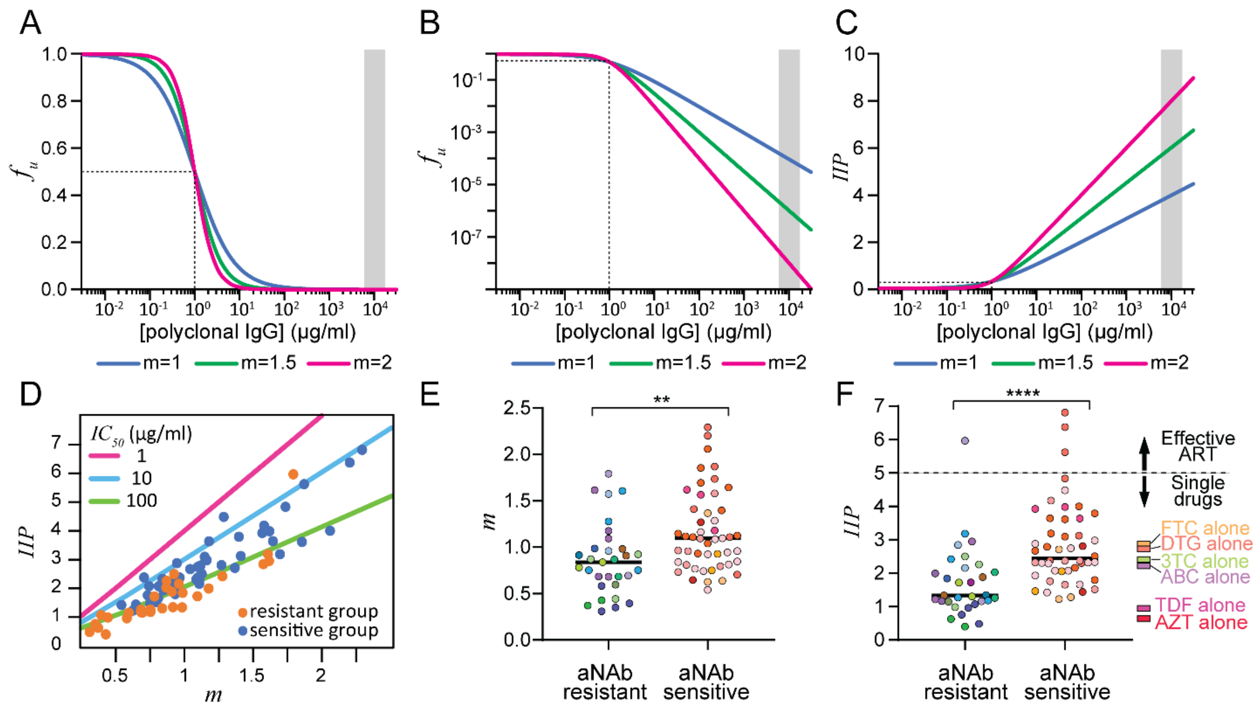

Figure 3. Inhibitory effect of aNAbs at physiologic IgG concentrations. (**A**) Hypothetical dose-response curves for inhibition of infection by autologous IgG antibodies. The fraction of infection events not inhibited (fraction unaffected or f_u) declines with increasing antibody concentrations. Curves show inhibition by three different antibody preparations that have the same IC_{50} (1 μg/ml, dotted line) but different slopes (*m*), a measure of cooperativity. In vitro neutralization assays are conducted at IgG concentrations well below physiologic IgG concentrations (shaded area). (**B**) Curves from (A) plotted with a logarithmic y-axis, illustrating the dramatic effect of *m* on inhibition. (**C**) Instantaneous inhibitory potential (IIP), the logs of inhibition of a single round of infection, for the same antibody preparations. (**D**) Effect of *m* on IIP for distinct isolates from the aNAb-resistant (orange, n = 31) and aNAb-sensitive (blue, n = 48) groups. IC_{50} value trend lines are shown at three indicated concentrations. For many resistant isolates, *m*, IC_{50} and IIP, could not be determined because infection did not consistently decrease with increasing IgG concentrations. (**E**) Distribution of slope values for the isolates from (D). Circles represent distinct isolates, and colors represent participant. Bar represents median. Significance was calculated using the Mann Whitney test. ** = P < 0.01 (**F**) Distribution of IIP values for the isolates from (D). Dotted line indicates the IIP value above which effective suppression of viral replication by combination ART regimens is observed (85). IIP values for single antiretroviral drugs at average plasma concentrations are shown (80, 85). Significance was calculated using the Mann Whitney test. **** = P < 0.0001

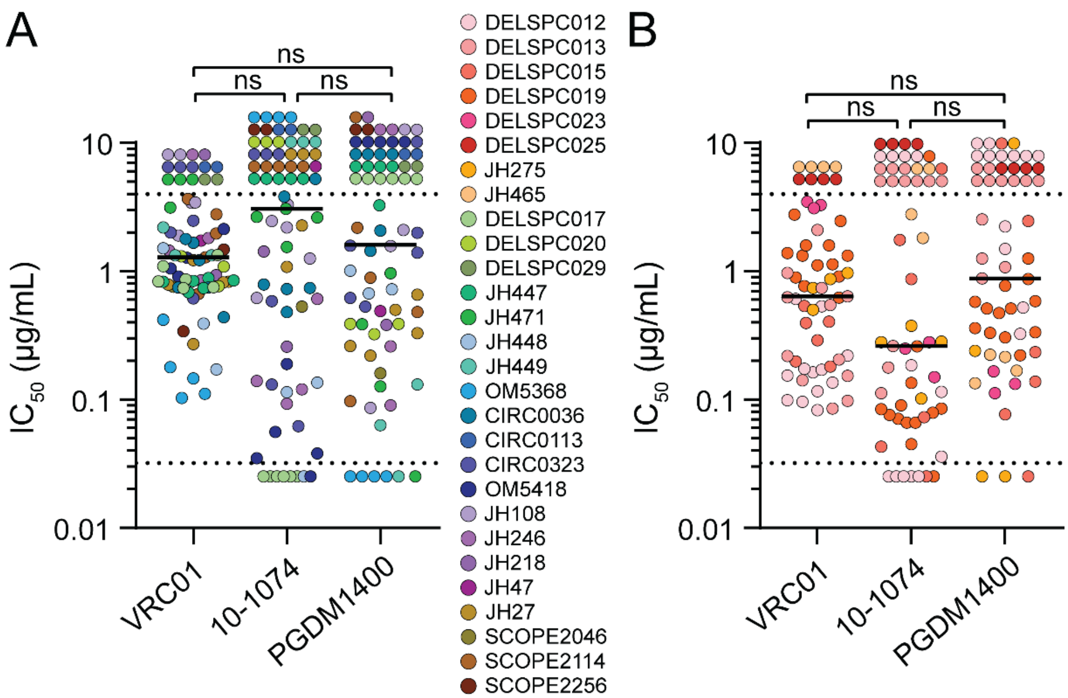

Figure 4. Sensitivity of outgrowth viruses to bNAbs. (**A**) TZM.bl-based neutralization assays were conducted with VRC01, 10-1074, and PGDM1400 and pseudoviruses generated from outgrowth viruses (n=74) from the aNAb-resistant group. (**B**) Neutralization assays with pseudoviruses generated from outgrowth viruses (n=58) from the aNAb-sensitive group. IC_{50} values above the highest antibody concentration tested are shown above the dotted lines at 4 µg/ml. Values below the lowest concentration tested are shown below the dotted lines at 0.032 µg/ml. Circles represent distinct isolates, and colors represent participants. We used a nonparametic one-way ANOVA (Friedman test) followed by Dunn's test for multiple comparisons to calculate significance. Bar represents median.

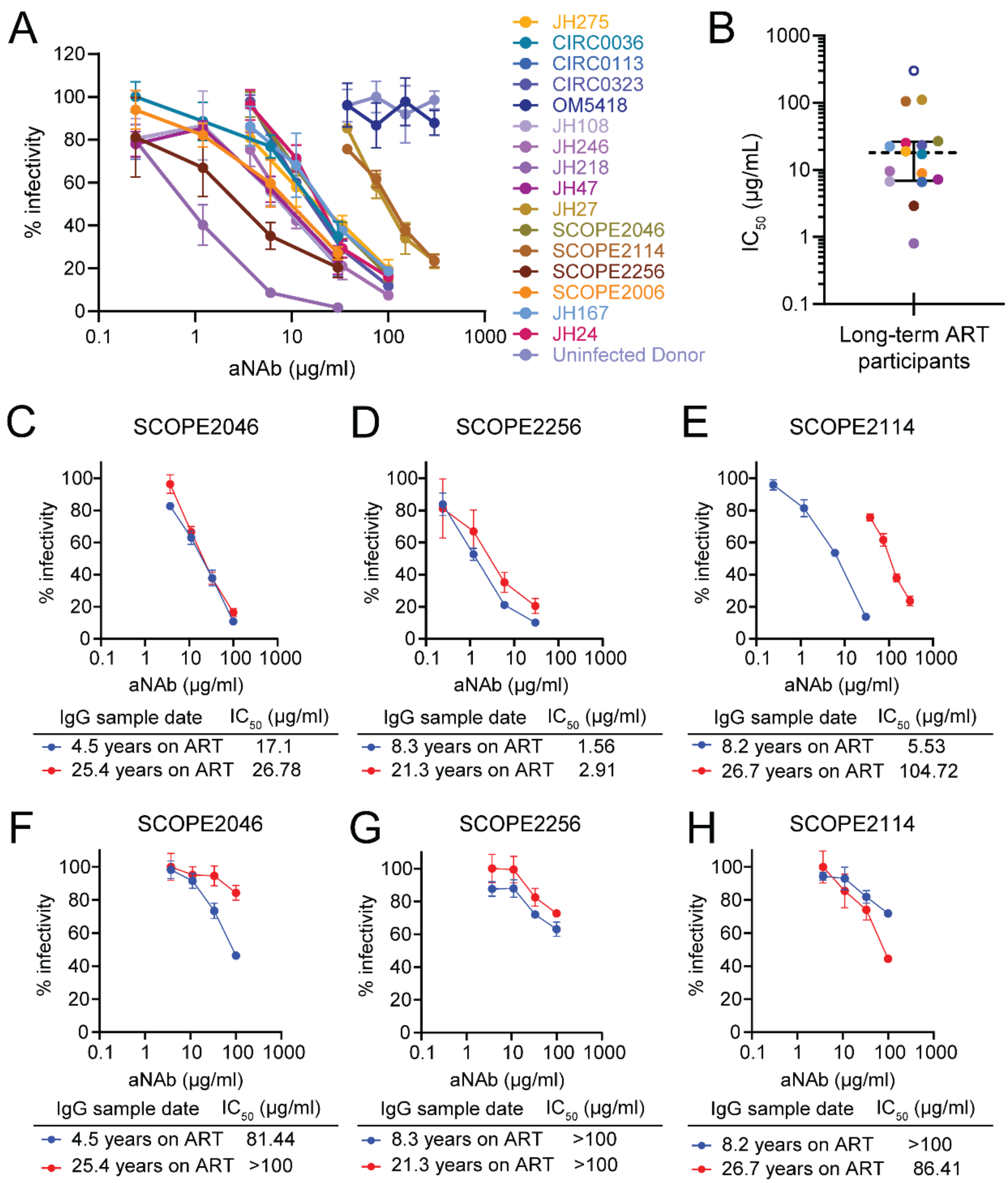

Figure 5. Persistence of neutralizing antibodies to HIV-1 Env in PWH on long-term ART. (**A**) Dose-response curves for inhibition of SF162 pseudovirus infection of TZM.bl cells by IgG purified from 16 PWH on long-term ART and one uninfected donor. (**B**) IC_{50} values from dose-response curves in (A). A value above the highest concentration tested (300 µg/ml) is shown in an open symbol. Dashed line represents median, and solid bars represent interquartile range. n = 16. (**C**) Dose-response curves for the inhibition of SF162 pseudovirus infection of TZM.bl by early and 20-year IgG samples from SCOPE2046, (**D**) SCOPE2256, and (**E**) SCOPE2114. (**F**) Dose-response curves for the inhibition of TZM.bl infectivity of one autologous outgrowth virus by early and 20-year autologous IgG collection timepoints from SCOPE2046, (**G**) SCOPE2256, and (**H**) SCOPE2114. Data for (A), (C), (D), (E), (F), (G), and (H) are reported as percentage (mean, SEM) of infectivity from triplicate measurements.

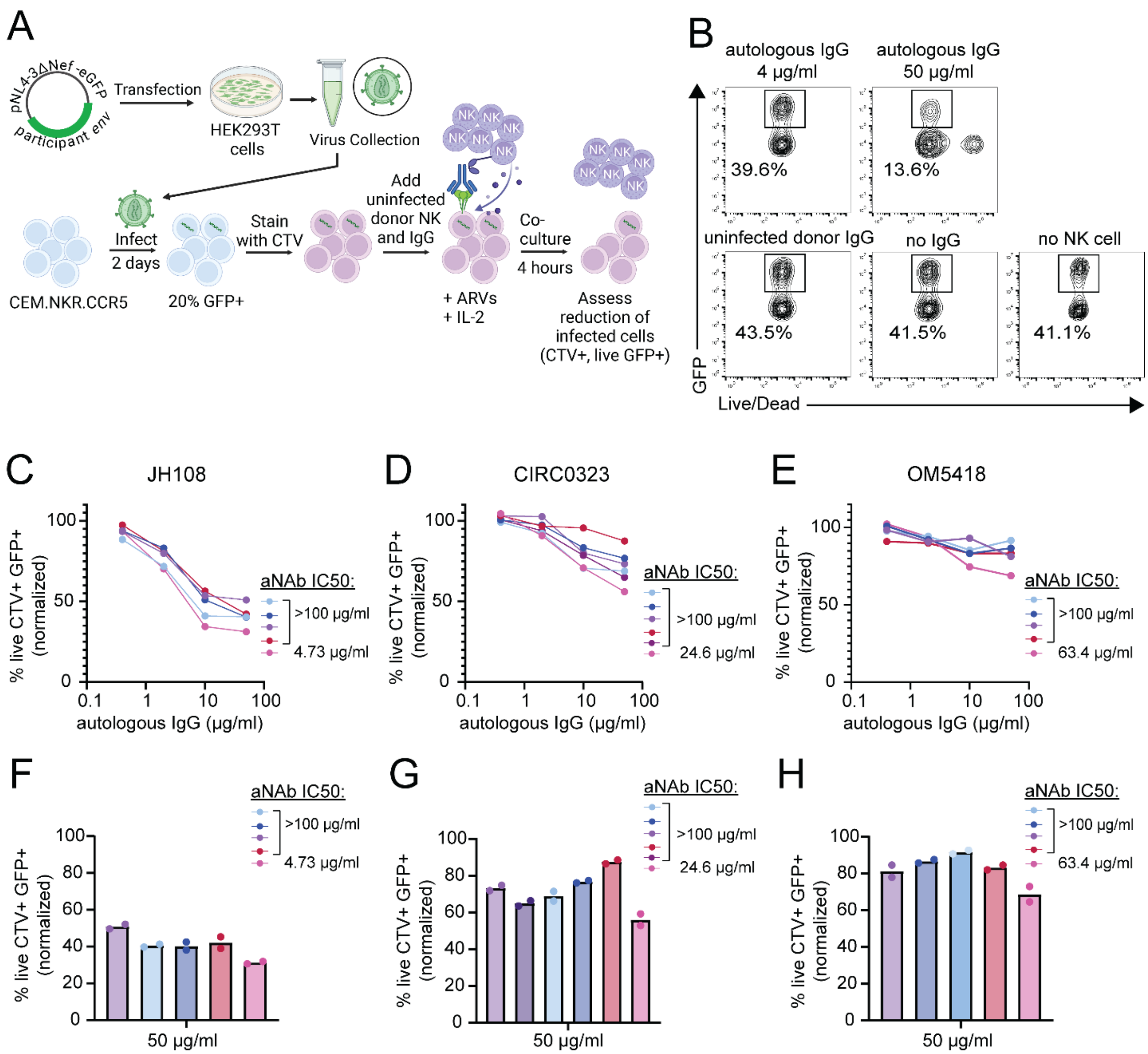

Figure 6. Cells infected with outgrowth viruses are susceptible to ADCC with autologous IgG obtained after long-term ART. (**A**) In vitro ADCC assay. Participant-specific *env* genes from outgrowth viruses were cloned into NL4-3-ΔNef-eGFP backbone to generate replication-competent reporter viruses. Target CEM.NKR.CCR5 cells (88) were infected with reporter viruses and after 2 days were stained with Cell Trace Violet (CTV). Target cells were co-cultured with uninfected donor NK cells and autologous IgG in the presence of antiretroviral drugs (ARVs) and IL-2 for four hours. The reduction of infected cells was assessed by flow cytometry. (**B**) Representative flow cytometry plots showing the percentage of live GFP+ CTV+ CEM.NKR.CCR5 target cells after co-culture with uninfected donor NK cells in the presence of the lowest (0.4 µg/ml) and highest concentration (50 µg/ml) of autologous IgG. Plots from control wells with uninfected donor IgG, without IgG, and without NK cells are shown. (**C, D, E**) For three long-term ART participants, measurements show the percentage of live GFP+ CTV+ CEM.NKR.CCR5 target cells after co-culture with uninfected donor NK cells in the presence of autologous IgG. Target cells were infected with GFP-reporter outgrowth viruses (one color each) and stained with CTV. aNAb-sensitive viruses are indicated in pink with the corresponding aNAb IC_{50} values, and aNAb-resistant viruses (IC_{50} values >100

μg/ml) are represented in other colors. Data are reported as a mean percentage of two replicates normalized to uninfected donor IgG. (**F, G, H**) Data from the highest autologous IgG concentration (50 μg/ml) in C, D, and E are replotted with the mean and two replicates shown. Colors correspond to the same viruses as in C, D, and E.

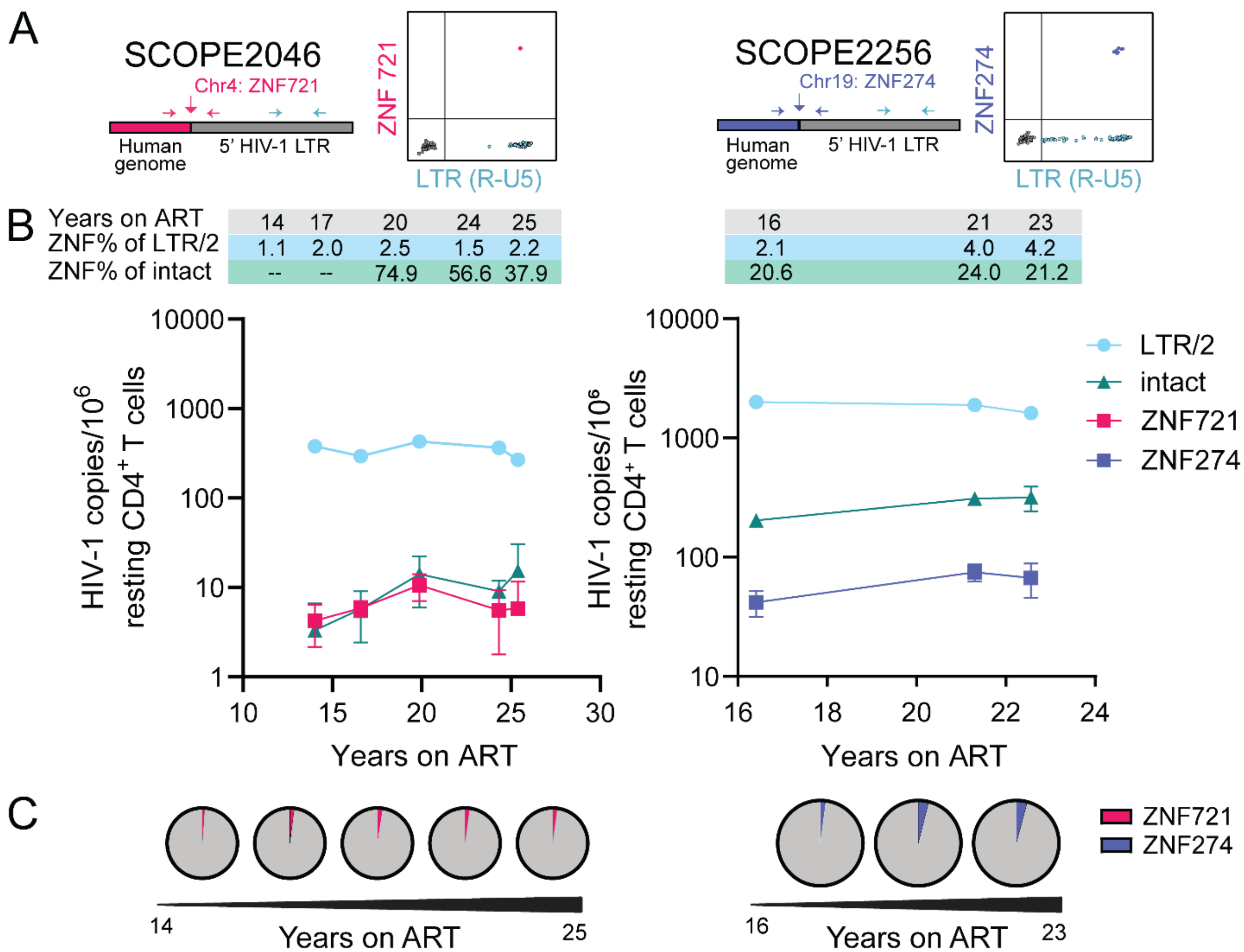

Figure 7. Persistence and prevalence of aNAb-resistant outgrowth clones integrated in ZNF regions. (**A**) Duplex ddPCR assays were designed to capture the frequency of proviruses with a specific integration site and *env* sequence matching an aNAb-resistant outgrowth clone. ddPCR plots display representative data from one well. (**B**) Longitudinal quantification of the SCOPE2046 ZNF721 and SCOPE2256 ZNF274 proviruses over time on ART. ZNF frequencies (pink or purple) and LTR/2 frequencies (blue) were determined by custom ddPCR assay. Intact proviral frequencies (green) were determined by IPDA (102). Data from 2-16 replicates are shown as proviral copies per 10^6 resting $CD4^+$ T-cells (mean, SEM) after correction for DNA shearing. ZNF percentages of LTR/2 and intact proviruses are shown above the graph at the corresponding time on ART. Dashes (--) represent ZNF frequencies larger than the intact proviral frequency. (**C**) Pie charts depicting proportion of ZNF721 (pink) or ZNF274 (purple) out of respective detected LTR/2 copies for each time point.

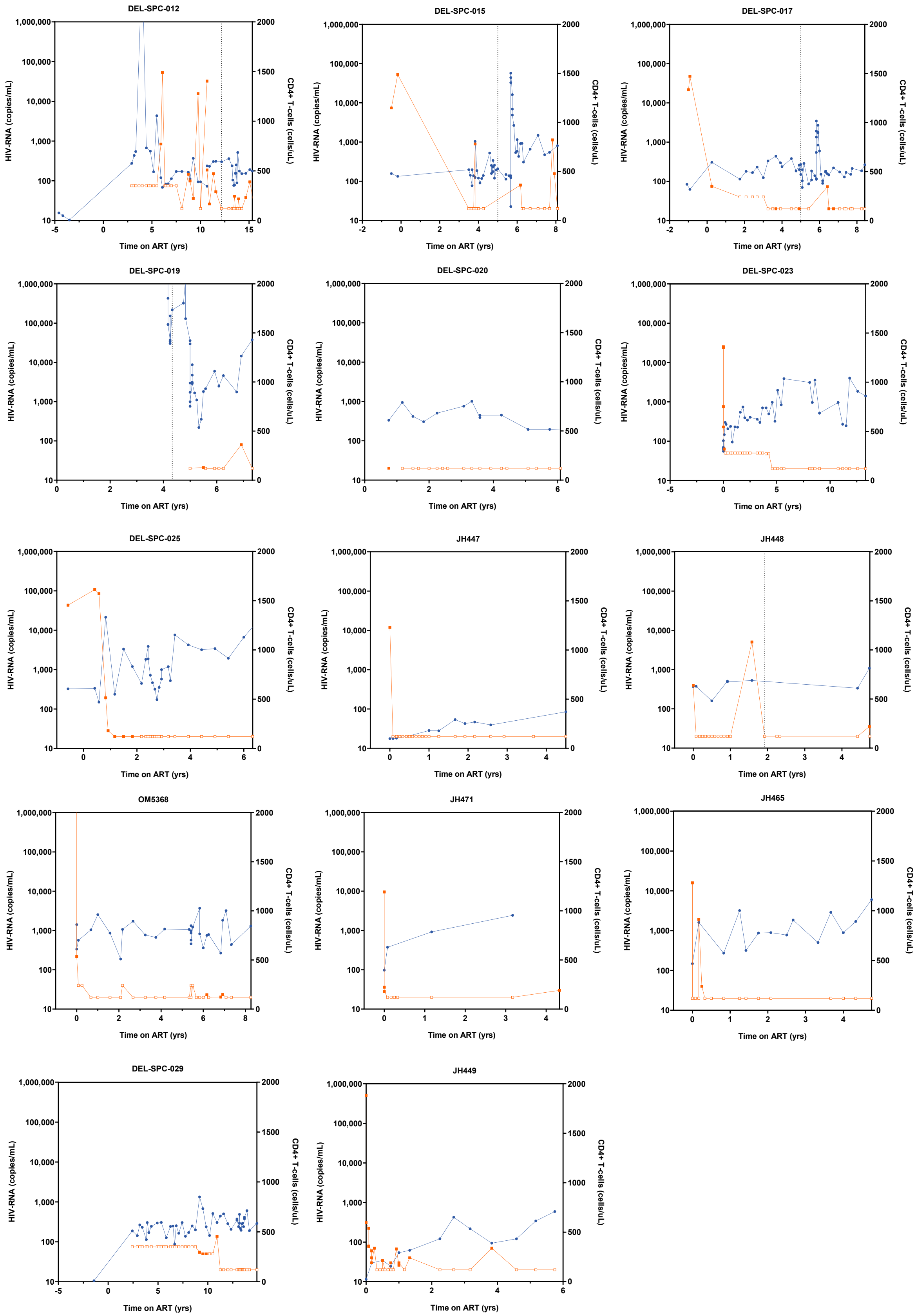
DEL-SPC-012
DEL-SPC-015
DEL-SPC-017
DEL-SPC-019
DEL-SPC-020
DEL-SPC-023
DEL-SPC-025
JH447
JH448
OM5368
JH471
JH465
DEL-SPC-029
JH449
HIV-RNA (copies/mL)
CD4+ T-cells (cells/uL)
Time on ART (yrs)
10
100
1,000
10,000
100,000
1,000,000
0
500
1000
1500
2000

Supplemental Figure 1. Plasma HIV-RNA levels and $CD4^+$ T cell counts of PWH on ART. Levels of plasma HIV-1 RNA (copies/mL) are plotted with solid orange squares and $CD4^+$ T cells (cells/µL) are plotted in blue circles against total time on ART. Time values <0 represent measurements taken before ART initiation. Plasma HIV-RNA values below the limit of detection of the assay are indicated in open orange squares. For DEL-SPC-015, -017, and -019, viral load measurements during VRC01 administration and an ATI in the ACTG trial A5340 (IDs A02, A06, and A13, respectively) are not displayed but can be found in Bar et al. (54). For DEL-SPC-012, -015, -017, -019, and JH448, dotted vertical lines represent the starting time of uninterrupted ART.

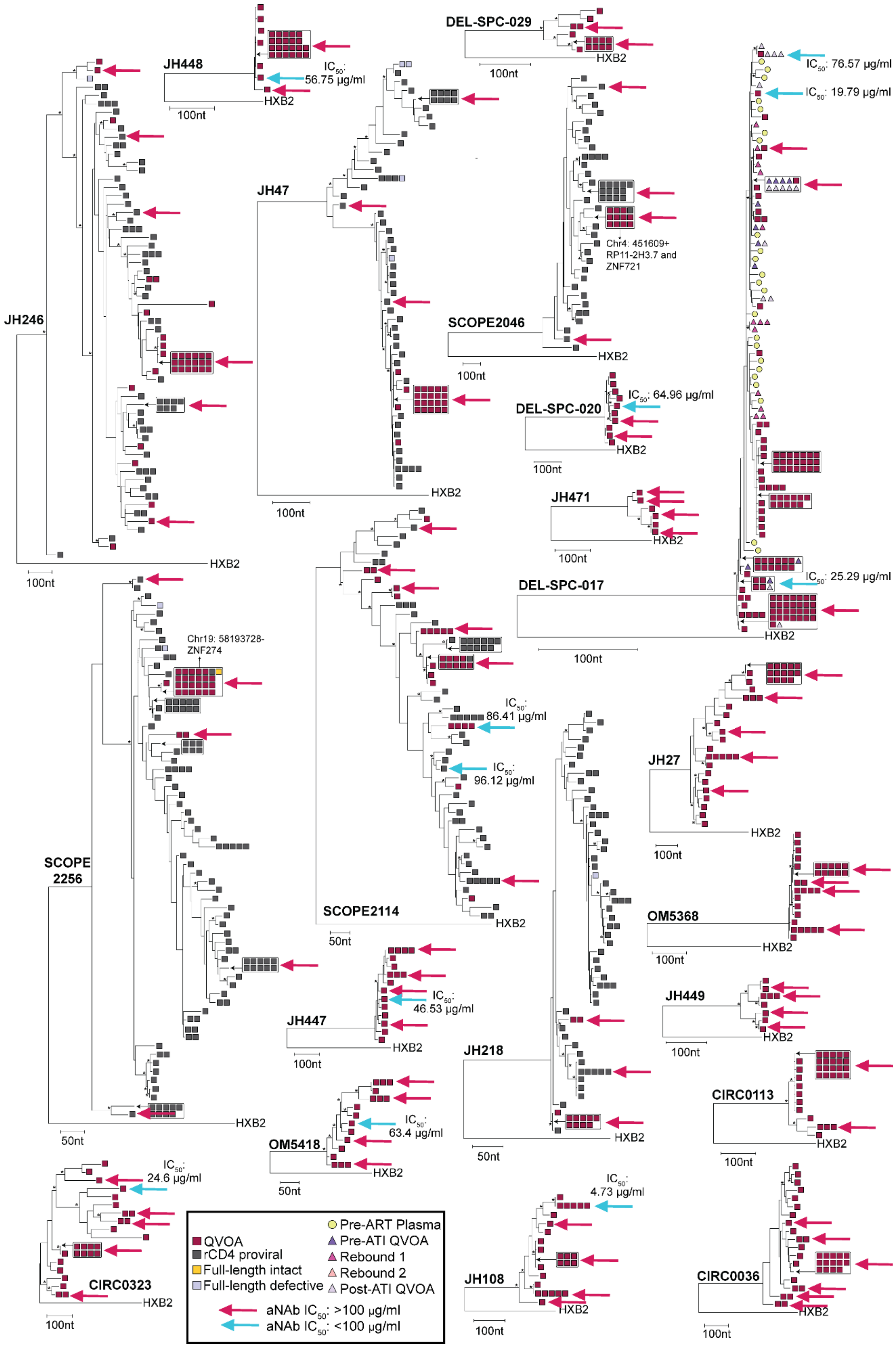
JH448
IC50: 56.75 µg/ml
HXB2
100nt
DEL-SPC-029
JH246
JH47
SCOPE2046
Chr4: 451609+ RP11-2H3.7 and ZNF721
IC50: 76.57 µg/ml
IC50: 19.79 µg/ml
DEL-SPC-020
IC50: 64.96 µg/ml
JH471
DEL-SPC-017
IC50: 25.29 µg/ml
SCOPE 2256
Chr19: 58193728-ZNF274
50nt
SCOPE2114
IC50: 86.41 µg/ml
IC50: 96.12 µg/ml
JH27
OM5368
JH218
JH447
IC50: 46.53 µg/ml
JH449
OM5418
IC50: 63.4 µg/ml
CIRC0113
CIRC0323
IC50: 24.6 µg/ml
JH108
IC50: 4.73 µg/ml
CIRC0036
QVOA
rCD4 proviral
Full-length intact
Full-length defective
Pre-ART Plasma
Pre-ATI QVOA
Rebound 1
Rebound 2
Post-ATI QVOA
aNAb IC50: >100 µg/ml
aNAb IC50: <100 µg/ml

Supplemental Figure 2. Neutralization by aNAbs for reservoir viruses of PWH in the aNAb-resistant group. Maximum likelihood phylogenetic trees of intact *env* sequences for participants are shown, with each tree rooted to HXB2. Single genome sequencing of *env* was performed on cDNA reverse-transcribed from extracted viral RNA from p24^{+} supernatants of QVOA wells (red squares) or on proviral DNA from resting CD4^{+} T cells (rCD4, grey squares). Near full-length genome sequences were obtained from the proviral DNA and are indicated as intact (yellow squares) or defective (blue squares). For DEL-SPC-017, who previously received VRC01 and an ATI in the ACTG trial A5340 (ID A06), sequences are displayed for pre-ART plasma (yellow circles), pre- and post-ATI QVOA samples (purple and lavender triangles), and rebound virus (red and pink triangles) (54, 61). Bootstrap values greater than 70% are denoted with an asterisk. Scale units are represented in nucleotides. Red arrows indicate proviruses resistant to neutralization by contemporaneous aNAbs with IC_{50} values >100 µg/ml. Blue arrows indicate proviruses sensitive to neutralization by aNAbs with IC_{50} values at the specified value <100 µg/ml. Chromosomal integration sites obtained by integration site loop amplification and corresponding gene name are indicated. Portions of the phylogenetic trees in this figure were modified from Bertagnolli et al. (30) and McMyn et al. (15).

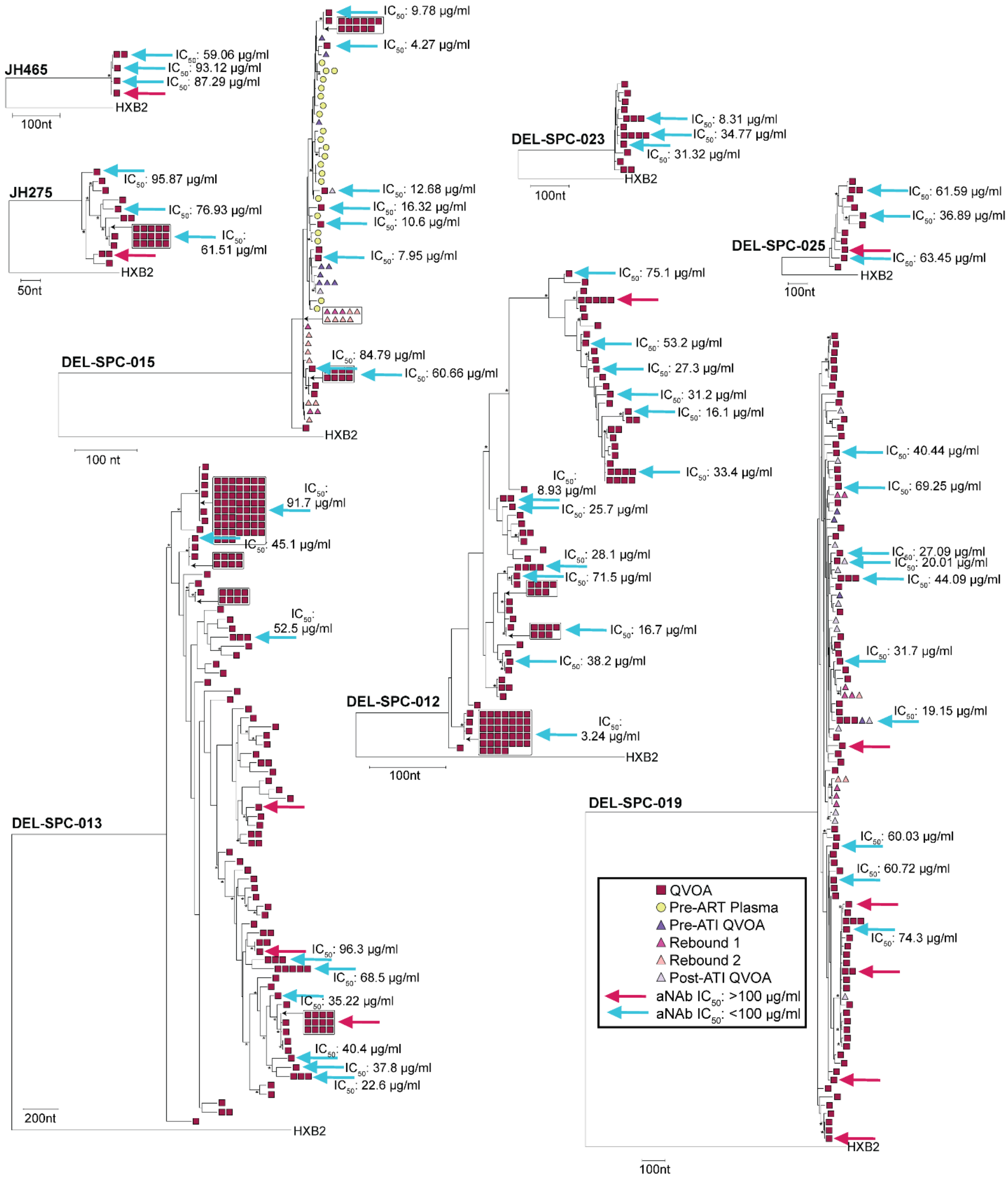

Supplemental Figure 3. Neutralization by aNAbs for reservoir viruses of PWH in the aNAb-sensitive group. Maximum likelihood phylogenetic trees of intact *env* sequences for participants are shown with each tree rooted to HXB2. Single genome sequencing of *env* was performed on cDNA reverse-transcribed from extracted viral RNA from p24⁺ supernatants of QVOA wells (red squares). For DEL-SPC-015 and -019, who previously received VRC01 and an ATI in the ACTG trial A5340 (IDs A02 and A13, respectively), sequences are displayed for pre-ART plasma virus (yellow circles), pre- and post-ATI QVOA samples (purple and lavender triangles), and rebound virus (red and pink triangles) (54, 61). Bootstrap values greater than 70% are denoted with an asterisk. Scale units are represented in nucleotides. Red arrows indicate proviruses resistant to neutralization by aNAbs with IC_{50} values >100 μg/ml. Blue arrows indicate proviruses sensitive to neutralization by aNAb with IC_{50} values at the specified value <100 μg/ml. Portions of the phylogenetic trees in this figure were modified from Bertagnolli et al. (30).

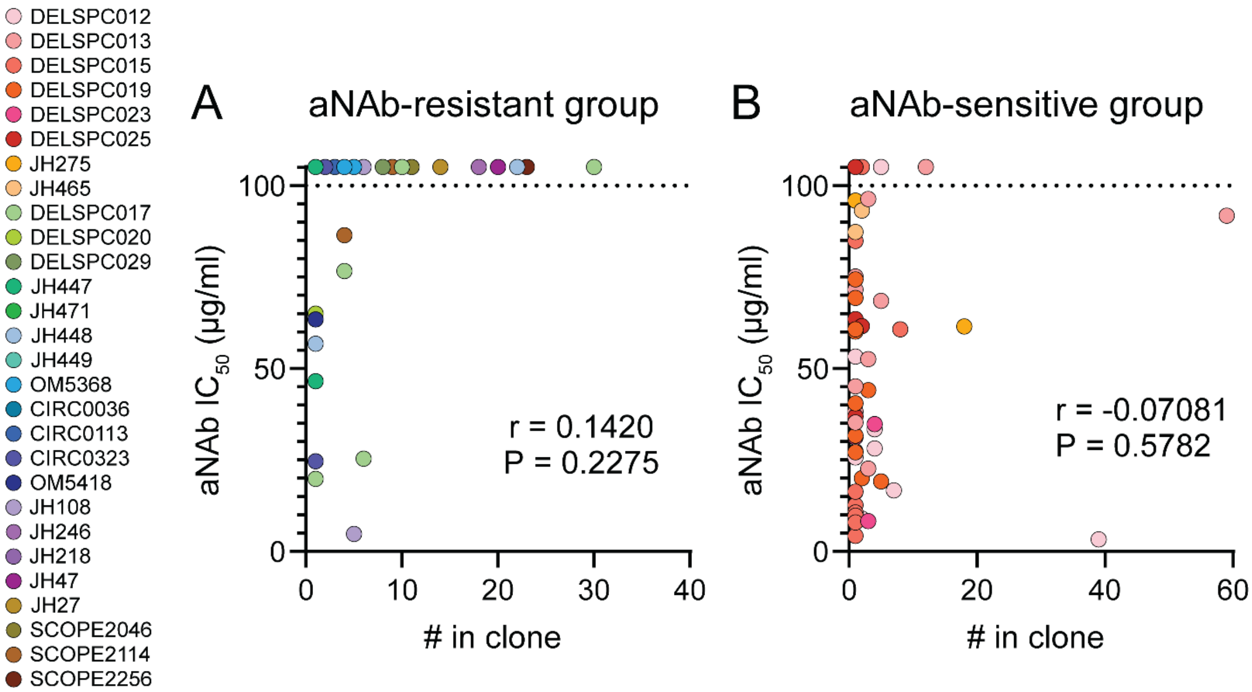

Supplemental Figure 4. No correlation between aNAb IC_{50} values and the number of isolates with identical *env* sequences. aNAb IC_{50} values for distinct isolates are replotted from Figure 2A for (**A**) the aNAb-resistant group (n = 74) and (**B**) the aNAb-sensitive group (n = 64) against the number of isolates with identical *env* sequences for the corresponding pseudovirus. Spearman's correlation values are shown.

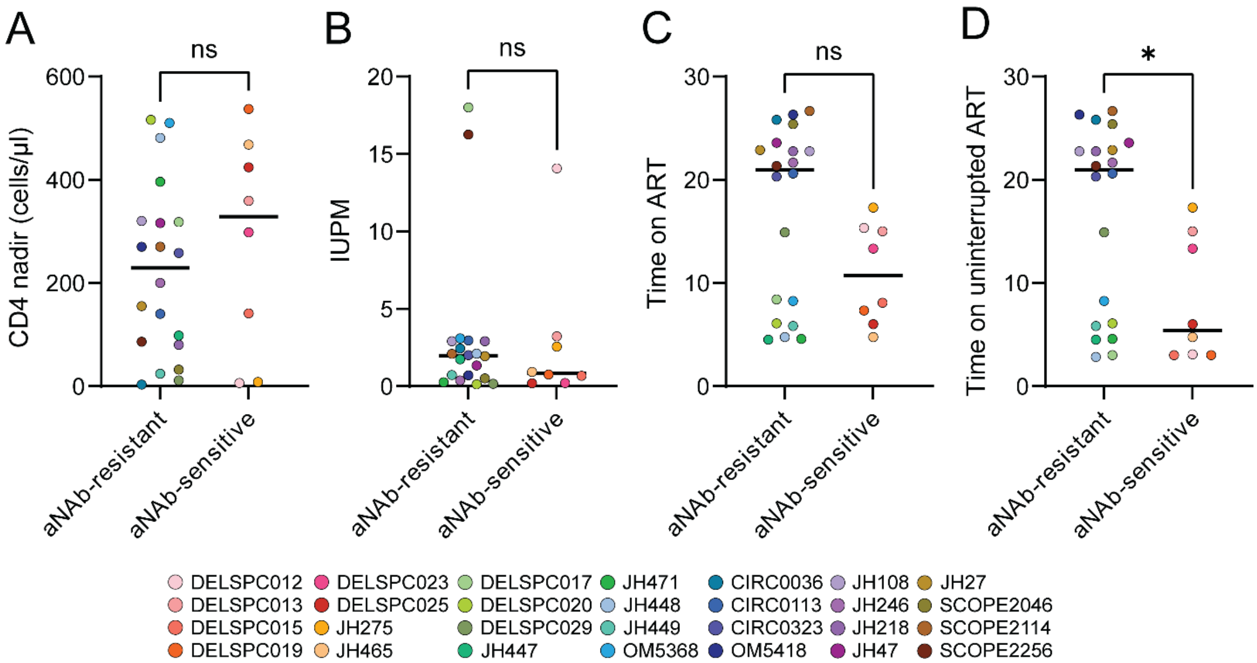

Supplemental Figure 5. Clinical history and reservoir characteristics compared between participants in the aNAb-resistant and aNAb-sensitive groups. Comparisons between aNAb-resistant group (n = 20 PWH) and aNAb-sensitive group (n = 8 PWH) values for (**A**) CD4 nadir, (**B**) IUPM, (**C**) time on ART, and (**D**) time on uninterrupted ART. Significance was calculated using the Mann Whitney test. * = P < 0.05.

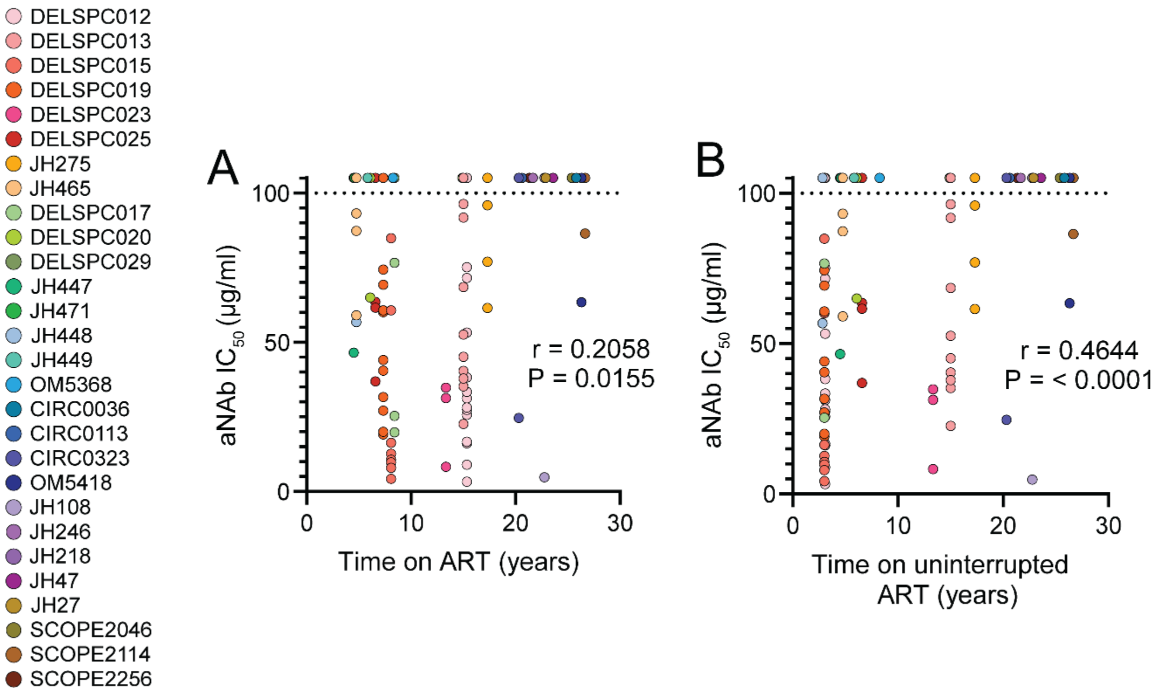

Supplemental Figure 6. Relationship between aNAb neutralization and time on ART. aNAb IC_{50} values from Figure 1A correlate with (**A**) total time on ART including short treatment interruptions (Spearman's correlation, n = 138) and (**B**) time on uninterrupted ART (Spearman's correlation, n = 138). Inclusion of multiple isolates from individual PWH give data points with the same x-axis values.

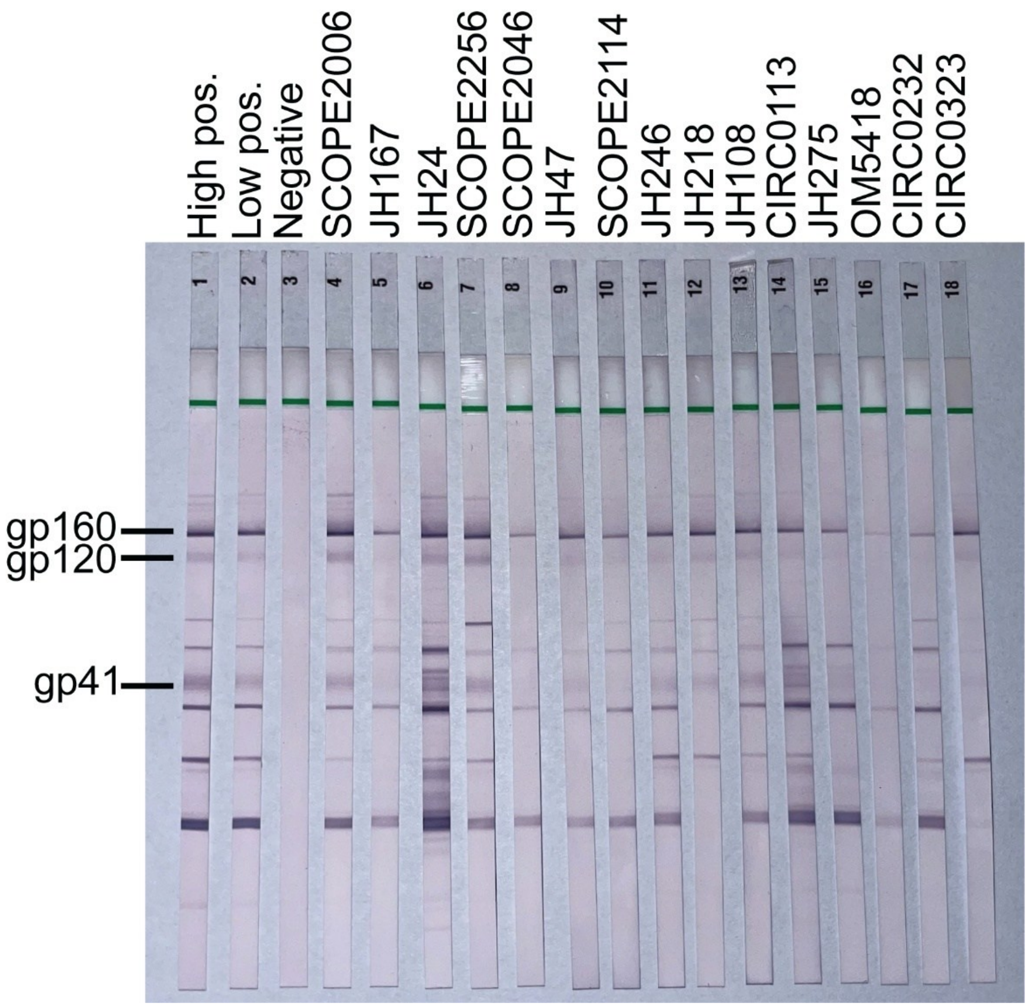

Supplemental Figure 7. HIV-1 western blot analysis of IgG purified from plasma of PWH on long-term ART. The first three columns are the high and low positive controls and the negative control. The following columns detect antibodies to HIV-1 for the indicated participants. Lanes 4-6 represent PWH with one or no outgrowth wells. Lanes 7-14, 16, and 18 represent PWH in the aNAb-resistant group. Lane 15 is a PWH in the aNAb-sensitive group. Lane 17 is a PWH on ART for over 20 years, initiating ART during acute infection and therefore excluded from this study. Bands for HIV-1 Env gp160, gp120, and gp41 are labeled.

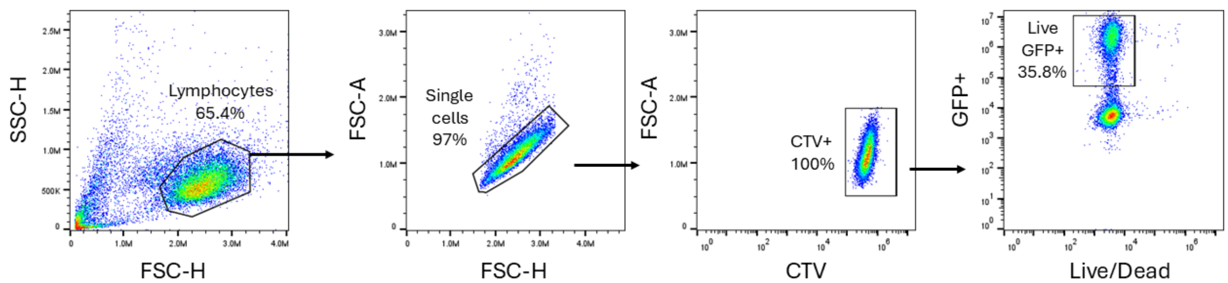

Supplemental Figure 8. Gating strategy for ADCC experiments illustrated using a representative control well with infected CEM.NKR.CCR5 cells and no NK cells. Gates were based on lymphocyte size (SSC-H, FSC-H) → single cells (FSC-A, FSC-H) → CTV$^+$ (FSC-A, CTV) → GFP$^+$, live (GFP, LIVE/DEAD Fixable Near-IR). From this analysis, we determined the percentage of CTV$^+$ single lymphocytes that were GFP$^+$ and viable: (viable,GFP$^+$CTV$^+$/CTV$^+$)*100. ADCC was assessed using this value normalized to the control wells with IgG from uninfected donors.

Supplemental Table 1. Characteristics of study participants.

ID	Age[A]	Sex	Race[B]	Time Since Diagnosis (Years)	Time on ART Regimen (years)	Current ART regimen[C]	CD4 nadir (cells/µl)	Plasma HIV-1 RNA (copies/mL)[A,D]
DEL-SPC-012[E]	46	M	B	21.0	15.3	ABC/DTG/3TC	6	<20
DEL-SPC-015[E]	50	M	B	8.5	8.1	ATV/r	141	<20
DEL-SPC-017[E]	57	M	B	9.5	8.4	BIC/FTC/TAF	318	<20
DEL-SPC-019[E]	51	M	B	7.4	7.3	BIC/FTC/TAF	537	<20
DEL-SPC-020[E]	34	M	B	7.1	6.1	ABC/DTG/3TC	516	<20
DEL-SPC-023[E]	51	F	B	14.6	13.3	BIC/FTC/TAF	298	<20
DEL-SPC-025[E]	42	M	B	6.6	6.0	EVG/c/FTC/TAF	424	<20
JH448	27	M	B	7.5	4.8	BIC/FTC/TAF	481	<20
JH447	32	M	B	4.5	4.5	BIC/FTC/TAF	98	<20
JH471	29	M	W	4.6	4.6	BIC/FTC/TAF	396	30
JH465	24	M	B	4.8	4.8	BIC/FTC/TAF	468	<20
JH449	35	M	B	5.8	5.8	BIC/FTC/TAF	24	<20
OM5368	60	M	W	8.3	8.3	BIC/FTC/TAF	510	<20
JH246	68	M	B	25.3	21.7	DTG/DOR	>200	<20
JH108	57	F	B	22.9	22.8	ABC/DTG/3TC	320	<20
JH47	48	M	B	30.4	23.6	BIC/FTC/TAF	316	<20
JH218	72	M	W	30.8	22.8	BIC/FTC/TAF	80	<20
JH27	68	F	B	28.8	22.9	ABC/DTG/3TC	155	<20
JH275	66	M	B	30.3	17.3	RPV/DTG	8	<20
SCOPE2046	56	M	PI	30.8	25.4	BIC/FTC/TAF, ECV	32	<30
SCOPE2256	67	M	W	36.7	21.3	DTG, RPV/TAF/FTC	86	<30
SCOPE2114	81	M	W	36.3	26.7	BIC/FTC/TAF	270	<30
CIRC0036	70	M	W	37.8	25.8	RPV/FTC/TAF/EVG/c	3	<20
OM5418	56	M	W	28.4	26.3	BIC/FTC/TAF/DOR	270	<20
CIRC0113	57	M	W	29.8	20.6	ABC/DTG/3TC	140	<40
CIRC0323	60	M	W	32.7	20.3	MVC/DOR/DTG	258	<40
DEL-SPC-013[E]	61	M	B	19.0	15.0	BIC/FTC/TAF	185	<20
DEL-SPC-029[E]	55	M	B	16.6	14.9	BIC/FTC/TAF	11	<20
JH24	62	M	B	29.8	19.1	DTG/RPV	286	<20
JH167	67	F	B	24.8	22.4	BIC/FTC/TAF	145	<20
SCOPE2006	71	M	W	27.4	25.7	FTC/TAF, DTG	9	<30
Mean	54			20.3	15.9		225	

[A]At most recent sample date.
[B]Black; W, White; H, Hispanic, PI, Pacific Islander.
[C]Abbreviations: 3TC, lamivudine; ABC, abacavir; ATV, Atazanavir; BIC, bictegravir; /c, cobicistat; DOR, doravirine; DTG, dolutegravir; ECV, entecavir; EVG, elvitegravir; FTC, emtricitabine; MVC, maraviroc; RPV, rilpivirine; /r, ritonavir; TAF, tenofovir alafenamide.
[D]Plasma HIV-1 RNA levels were measured using the Hologic Aptima and Cobas assays.
[E]Denotes participants that were included in the prior study (30).

Supplemental Table 2. Isolates with IIP > 5.

Donor_Isolate	Group	Hill coefficient[A] (m)	IC_{50}[A](μg/ml)	IIP[B]	# of identical isolates	Years on uninterrupted ART
DEL-SPC-015_UD.B32	sensitive	2.20	12.68	6.37	1	3
DEL-SPC-015_UD.B18	sensitive	2.29	10.6	6.81	1	3
DEL-SPC-015_ST.A03	sensitive	1.87	9.78	5.62	1	3
JH108_A03	resistant	1.79	4.73	5.96	5	22.75

[A]Determined using the median effect equation (83).
[B]IIP of aNAbs at 10 mg/ml

Supplemental Table 3. Variable sensitivity of isolates from the aNAb-resistant group to neutralization by bNAbs.

Donor_Isolate	aNAb IC_{50} (µg/ml)	bNAb IC50 (µg/ml)		
		VRC01	10-1074	PGDM1400
JH108_A03	4.73	1.9	1.26	>4
DEL-SPC-017_ABB18	19.79	0.746	0.004	>4
CIRC0323_B46	24.6	>4	>4	0.531
DEL-SPC-017_ABB21	25.29	1.093	0.01	>4
JH447_B29	46.531	0.732	>4	>4
JH448_A07	56.75	0.172	0.114	0.726
JH5418_A14	63.4	1.27	0.038	>4
DEL-SPC-020-UDA19	64.96	1.09	>4	0.388
DEL-SPC-017_STC04	76.57	0.824	0.008	>4
SCOPE2114_B21	86.41	1.29	4	>4
DEL-SPC-017_STC11	>100	1.336	0.012	>4
DEL-SPC-017_STA01	>100	0.867	0.007	>4
DEL-SPC-017_ABB17	>100	0.731	<0.032	>4
DEL-SPC-020_STA10	>100	1.31	>4	0.323
DEL-SPC-020_STA13	>100	0.76	>4	0.39
DEL-SPC-029_ABB53	>100	>4	>4	>4
DEL-SPC-029_STB57	>100	>4	>4	>4
SCOPE2256-A15	>100	0.34	>4	>4
SCOPE2256-A24	>100	1.48	>4	>4
JH47_A07	>100	1.74	>4	0.49
SCOPE2046-A24	>100	0.75	0.53	0.16
JH246_A34	>100	1.82	0.12	>4
JH246_A22	>100	>4	0.093	0.09
JH246_A03	>100	1.45	0.61	>4
JH246_A01	>100	0.85	0.14	0.26
JH218_A09	>100	0.93	0.258	>4
JH218_A03	>100	>4	1.43	0.382
SCOPE2114_B42	>100	0.66	>4	2.19
SCOPE2114_B06	>100	1.97	>4	0.097
SCOPE2114_B01	>100	2.78	>4	0.89
SCOPE2114_B09	>100	3.42	>4	0.39

JH108_A04	>100	>4	2.2	2.1
JH108_A02	>100	3.66	0.62	>4
JH108_A14	>100	>4	2.46	0.086
JH108_A01	>100	3.45	3.31	1.57
CIRC0113_A03	>100	>4	>4	>4
CIRC0113_A09	>100	>4	>4	>4
OM5418_A03	>100	2.14	0.19	>4
OM5418_A10	>100	0.91	0.035	>4
OM5418_B39	>100	1.05	<0.032	>4
OM5418_A07	>100	0.42	0.056	>4
CIRC0323_A06	>100	>4	0.131	1.13
CIRC0323_A05	>100	2.48	0.586	1.58
CIRC0323_B03	>100	>4	>4	1.61
CIRC0323_B18	>100	0.61	>4	>4
CIRC0323_A08	>100	2	0.062	0.621
JH27_A04	>100	0.78	>4	0.5
JH27_A09	>100	0.821	>4	0.261
JH27_A11	>100	0.27	1.08	0.266
JH27_A21	>100	0.81	>4	0.22
JH27_B22	>100	1.22	2.28	0.531
CIRC0036_A13	>100	1.22	3.81	1.44
CIRC0036_A16	>100	0.44	0.74	>4
CIRC0036_B13	>100	1.67	0.79	>4
CIRC0036_B17	>100	1.79	>4	2.08
CIRC0036_B51	>100	0.74	0.48	>4
CIRC0036_C02	>100	0.74	0.73	>4
JH448_A02	>100	0.391	0.136	0.671
JH448_B07	>100	1.513	<0.032	1.008
JH447_B04	>100	0.82	>4	>4
JH447_B13	>100	0.679	>4	>4
JH447_B18	>100	0.885	>4	>4
JH447_B34	>100	0.842	>4	3.26
OM5368_A05	>100	0.111	>4	<0.032
OM5368_A07	>100	0.179	>4	<0.032
OM5368_A09	>100	0.146	>4	<0.032

OM5368_B04	>100	0.103	>4	<0.032
JH471_A07	>100	>4	2.63	<0.032
JH471_A08	>100	>4	1.55	0.127
JH471_A10	>100	>4	2.66	0.387
JH471_B08	>100	3.136	3.073	0.966
JH449_B05	>100	1.33	>4	0.106
JH449_B25	>100	2.195	>4	0.063
JH449_C02	>100	1.33	>4	<0.032

<0.032 >4 µg/ml